

## Polarization Structures in the Canadian Galactic Plane Survey: A Multispectral View

Roland Kothes<sup>1,2</sup> and T. L. Landecker<sup>1</sup>

<sup>1</sup>National Research Council of Canada, Herzberg Institute of Astrophysics, Dominion Radio Astrophysical Observatory, P.O. Box 248, Penticton, British Columbia, V2A 6J9, Canada

<sup>2</sup>Department of Physics and Astronomy, University of Calgary, 2500 University Drive N.W., Calgary, AB, Canada

**Abstract.** The comparison of structures, linearly polarized at 1420 MHz, with images in Stokes I, observations at other frequencies, and other sources can help us to learn more about the nature of these objects. We can distinguish between actual emission structures and those that merely affect the smooth background polarization by Faraday Rotation, the so-called Faraday screens. We can also gain more information about electron density and/or magnetic field enhancements that cause the Faraday Rotation and the distances to these objects.

### 1 The Polarization Horizon

As defined by Uyaniker et al. (2003) the ‘‘Polarization Horizon’’ is the maximum distance from which radio polarization is still detectable; more distant emission is depolarized by Faraday Rotation effects. This horizon affects Galactic background polarization as well as emission from supernova remnants, and from ‘‘Faraday screens’’ that exhibit themselves by changing the polarization angle of emission structures behind them. There are two different depolarization effects, depth depolarization and beam depolarization. In depth depolarization, polarized photons generated along the line of sight with the same polarization angle cancel each other because one has been Faraday-rotated by 90° before it reaches the other. In beam depolarization, polarized photons generated within the beam of the observations are Faraday-rotated differently along the line of sight and the net polarization level is reduced by averaging of vectors. Both effects depend on the electron density along the line of sight, but, while depth depolarization arises mainly from a uniform magnetic field, beam depolarization is determined by the random field component. From the study of Brown et al. (2001) we know that in the area of the Canadian Galactic Plane Survey (CGPS, Taylor et al., 2003) the random magnetic field is not isotropic but is aligned with the uniform field. Hence to a first approximation we can calculate the Polarization Horizon as the distance from which a polarization vector is rotated by 90° by Faraday Rotation. For the CGPS at a frequency of 1420 MHz this requires a rotation measure of about  $RM = 36 \text{ rad m}^{-2}$ . The rotation measure is defined by:

$$RM = 0.81 \int_l B_{\parallel}(l) n_e(l) dl \approx 0.81 \overline{B_{\parallel}} DM \quad (1)$$

Here  $B_{\parallel} \approx \sin \ell B_{\text{tot}}$  is the magnetic field strength parallel to the line of sight,  $n_e$  the electron density,  $l$  the path length, and DM the dispersion measure, which we take from the Taylor & Cordes (1993) model of free electrons. With three different values for the total magnetic field  $B_{\text{tot}}$  (from the top: 0.5, 0.75, and 1.0  $\mu\text{G}$ ) we derive polarization horizons as displayed in Fig. 1 as gray lines. Interesting is the fact that for longitudes  $\ell$  lower than about 130° the Polarization Horizon remains more or less constant for a magnetic field strength above 0.75  $\mu\text{G}$ . Towards the anti-centre the horizon goes to infinity because we are looking almost perpendicular to the magnetic field lines.

We can locate the Polarization Horizon by examining supernova remnants (SNRs) and H II regions over an extended area. SNRs that are polarized should be closer than the Polarization Horizon, and vice versa. H II regions that are closer than the polarized emission will generally depolarize it (through beam

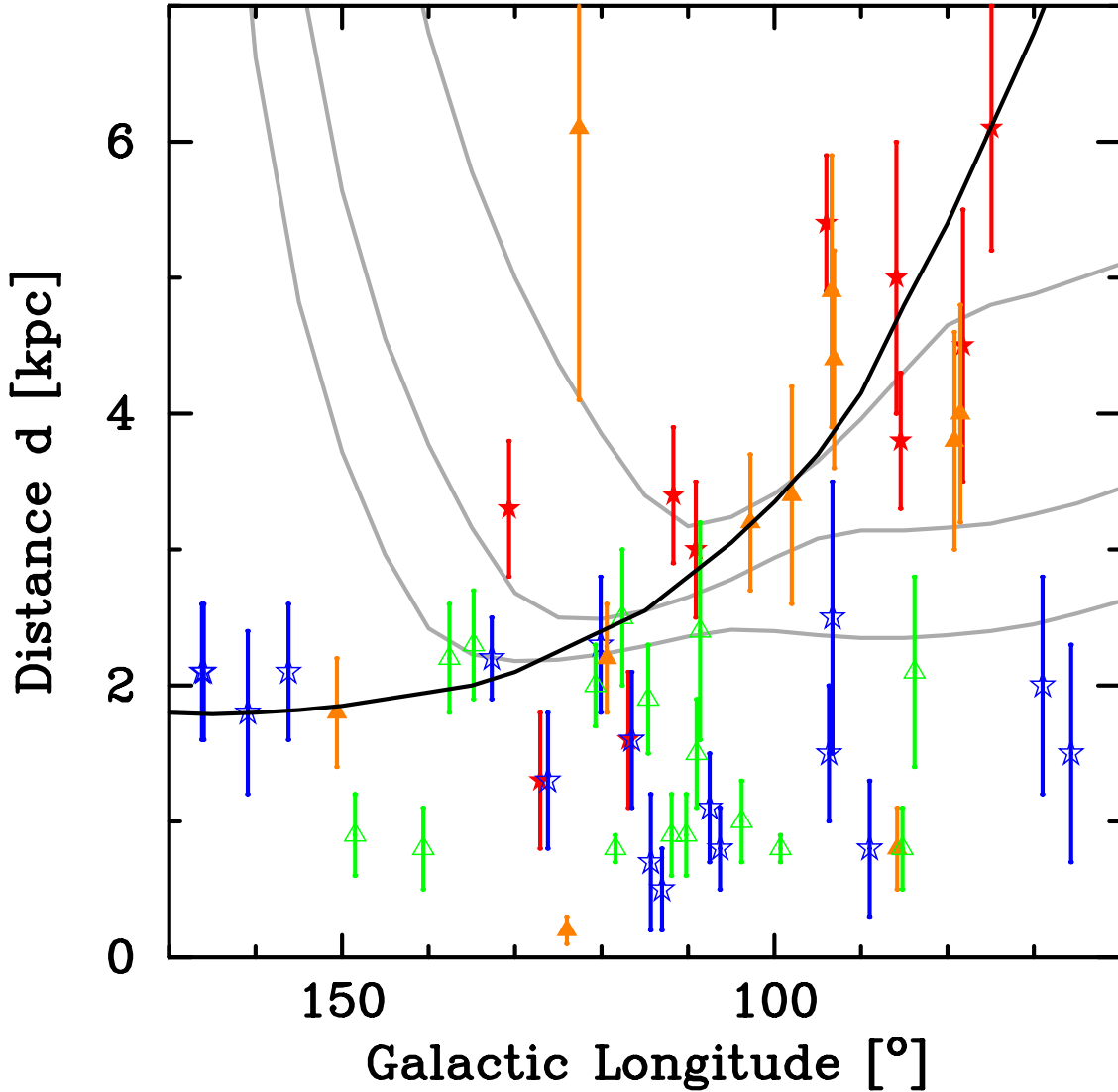


**Fig. 1.** Longitude-distance diagram covering most of the Canadian Galactic Plane Survey. The black solid line marks the maximum electron density in the Perseus arm (taken from Taylor & Cordes 1993). The gray solid lines mark an approximation for the Polarization Horizon for three different total magnetic field strengths, from the top: 0.5, 0.75, and 1.0  $\mu\text{G}$  (see text). Blue open stars mark SNRs which are polarized in the CGPS at 1420 MHz and red filled stars are unpolarized SNRs. Green open triangles mark H II regions that affect superposed polarization structures and orange filled triangles those H II regions that do not affect any superposed polarization structures.

depolarization in the dense and turbulent ionized gas), and those that have no perceptible effect on the polarized background will generally lie beyond the Polarization Horizon. We investigated the majority of SNRs and H II regions in the area covered by the CGPS. All SNRs that appear polarized (blue open stars in Fig. 1) are closer than about 2.5 kpc. All SNRs further away than 3 kpc are unpolarized (red filled stars). There are two nearby SNRs which are unpolarized, probably due to internal effects. H II regions that affect superposed polarization structures (green open triangles) are also located closer than about 2.5 kpc and all those beyond that distance do not affect background polarization (orange filled triangles). Together this evidence indicates that all polarization structures observable in the CGPS are generated and/or Faraday rotated closer than 2.5 kpc. There are closer H II regions that do not affect superposed polarization structures, which simply indicates that those particular structures are created closer to us than the H II regions. From this we can estimate a Polarization Horizon between

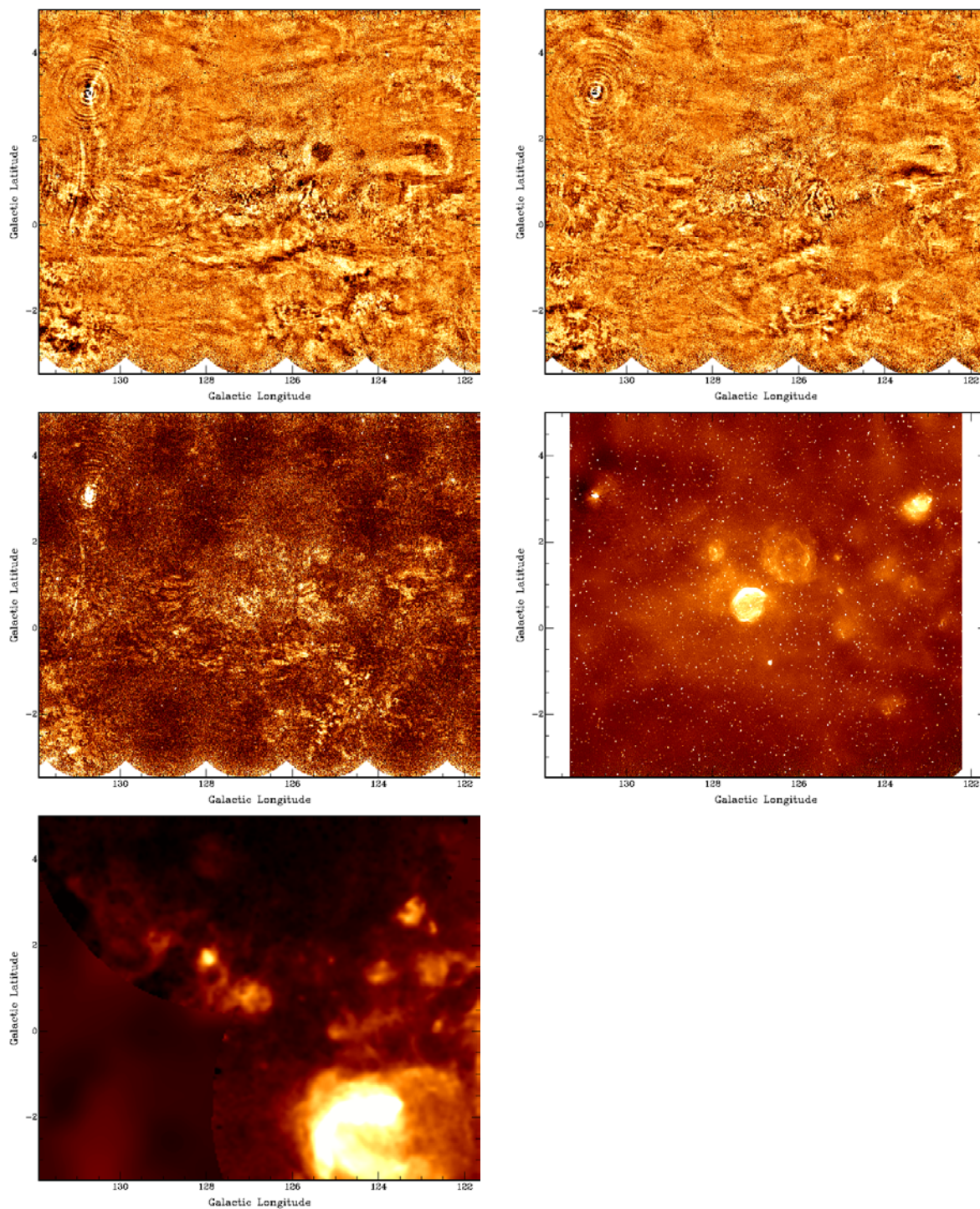


**Fig. 2.** Images of the area around the H II region Sh 2-185, taken from the Canadian Galactic Plane Survey. Displayed are Stokes Q (top left), Stokes U (top right), polarized intensity (middle left), and Stokes I (middle right) at 1420 MHz. The lower left panel shows the H $\alpha$  image.

2.5 and 3.0 kpc for longitudes lower than  $140^\circ$  and a mean magnetic field strength of about  $1 \mu\text{G}$ . The Polarization Horizon passes through the Perseus arm (whose centre is indicated by the black solid line) between  $\ell = 110^\circ$  and  $140^\circ$  which also means that at lower longitudes observed polarization structures

are most likely local. Unfortunately we cannot test whether the horizon moves towards infinity in the anti-centre because in this region of our Galaxy there are no distant sources available.

The most spectacular of the nearby H II regions that do not display any effect on superposed polarization structures is Sh 2-185 at a Galactic Longitude of  $\ell = 124^\circ 0$  and a Galactic Latitude of  $b = -1^\circ 9$  (Fig. 2). This source is located at a distance of about 200 pc. In Fig. 2 we clearly see polarization filaments and blobs overlapping with the position of the H II region (which is best visible in H $\alpha$  in the lower panel). These filaments are very prominent in Stokes Q and U and also in polarized intensity. Only a few faint structures coinciding with the H II region are visible in the Stokes I image. No synchrotron emission that might coincide with the polarization structures is detected. Some of the polarization filaments or structures pass right across Sh 2-185 without showing any effect. An H II region like this should completely depolarize background emission. This means that the polarization structure we see superposed on it must be generated between Sh 2-185 and us, and, if it is a Faraday screen, the smooth polarized emission that is rotated by this screen must also be generated within 200 pc. Another remarkable fact is that there is no diffuse synchrotron emission generated between the polarization horizon and Sh 2-185. If there were, it should be depolarized and we would see the impact of the H II region as a polarization structure (the smooth polarized background is hidden since the short spacings are missing from the polarization data).

## 2 A region of multiple polarization structures near $\ell = 165^\circ$

In Figure 3 images of an area of about  $10^\circ \times 7^\circ$  around Galactic Longitude  $165^\circ$  are displayed at various frequencies. Multiple polarization structures are visible on all scales in the Stokes Q and U images. There are three well-known SNRs in this area. All are bright radio and H $\alpha$  sources and all are at least partly polarized (HB 9 at  $\ell = 160^\circ 9$   $b = 2^\circ 6$ , VRO 42.05.01 at  $\ell = 166^\circ 0$   $b = 4^\circ 3$ , and OA 184 at  $\ell = 166^\circ 2$   $b = 2^\circ 5$ ).

In this section we will discuss (a) the two large polarization bubbles best seen in the Stokes Q and U images and (b) the depolarization structure seen near  $0^\circ$  latitude covering the longitude range from  $160^\circ$  to  $168^\circ$ , seen most clearly in polarized intensity. The latter separates the bubble structures in the north from the smooth bright polarization patches in the south. The smaller bubble covers a longitude range from  $164^\circ$  to  $167^\circ 5$  and latitude range from  $-2^\circ$  to  $+2^\circ$ . The larger bubble seems to surround the smaller one, but we see only the upper half. It starts at a longitude of  $161^\circ 5$  and continues at the high longitude edge of the image. This half-bubble starts at about  $0^\circ$  latitude and is detectable up to about  $4^\circ 5$ .

The depolarization structure in the middle of the images does not have a counterpart in radio-continuum Stokes I, but there is a rather bright H $\alpha$  filament which coincides with it. This H $\alpha$  filament seems to continue in a half-circle to the north and partly overlaps the emission from the SNR HB 9 without having any other noticeable radio polarization structure. This depolarization filament seems to reduce polarized emission superposed on it. In particular the polarization bubbles seem to stop just north of it, and at least the inner bubble continues to the south. This filament is apparently a foreground object, depolarizing background emission because of an enhanced electron density, as indicated by the bright H $\alpha$  emission. The continuing half-circle to the north is not visible in polarization because there is no background emission available. The most likely explanation for this is that a massive star in the centre has created an expanding shell of ionized electrons that is Faraday rotating background polarization structures.

The inner bubble is centred at about  $\ell = 165^\circ 5$  and  $b = 0^\circ$  and has a radius of around  $4^\circ$ . This object is very prominent in Stokes Q and U and also in polarized intensity. There is a faint diffuse shell of Stokes I radio continuum emission coinciding with this structure, indicating that the object is actually a synchrotron emitter rather than a Faraday screen rotating smooth Galactic background polarization. If this is a Faraday screen, the emission seen in Stokes I would have to be thermal, in which case it should be very bright in H $\alpha$ . However, in the H $\alpha$  image there is a bright filament just *outside* the north-eastern part of the shell. Together, this implies that this source is a SNR which is located behind the horizontal filament which is partly depolarizing its emission. The smooth faint structure of the radio-continuum shell indicates an early phase of evolution in which the shock wave

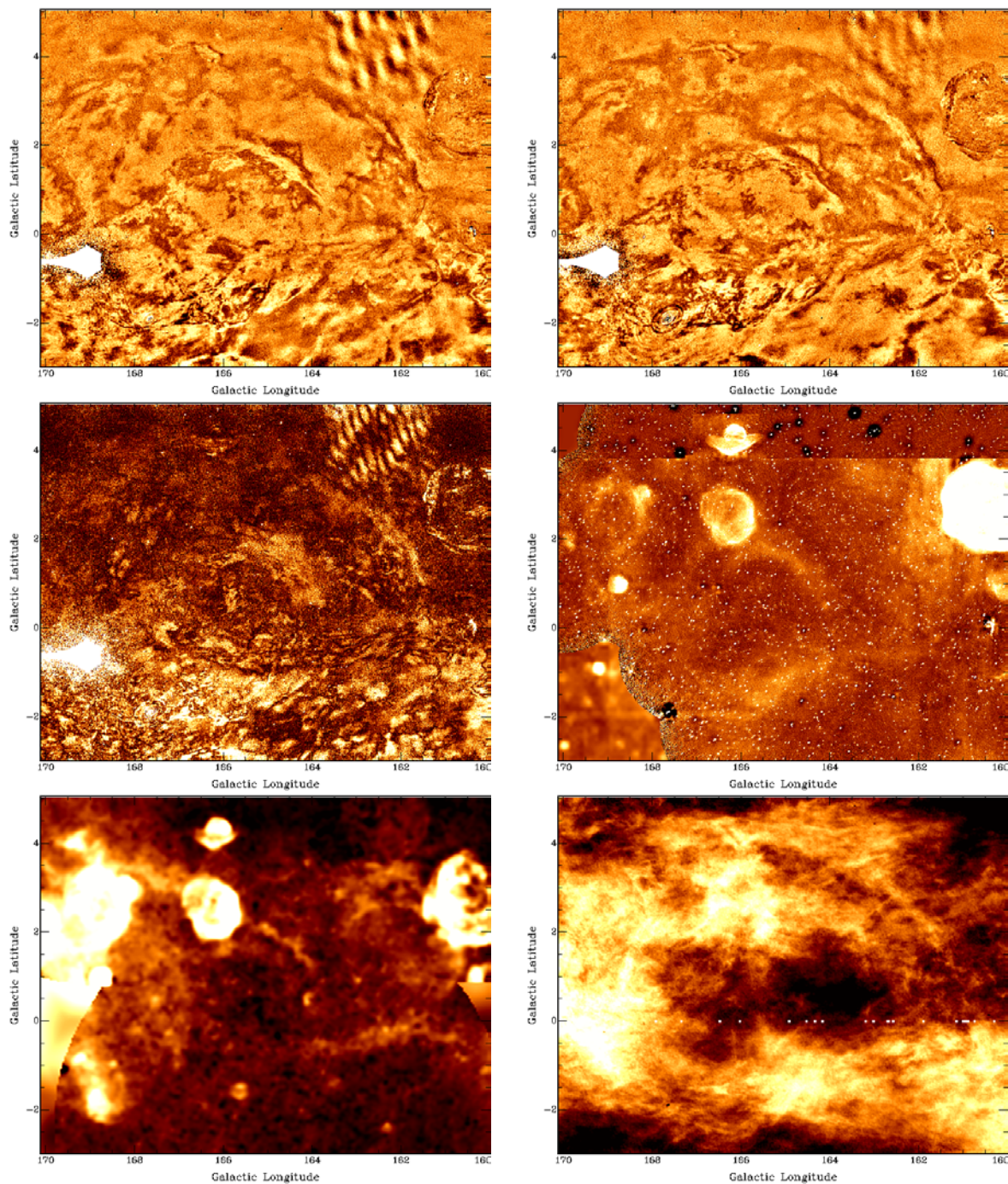


**Fig. 3.** Images of an area around Galactic Longitude  $165^\circ$ . Displayed are Stokes Q (top left), Stokes U (top right), polarized intensity (middle left), and Stokes I (middle right) at 1420 MHz taken from the Canadian Galactic Plane Survey. In the lower panels an  $H\alpha$  image is shown on the left and an H I image from the CGPS is shown on the right. The somewhat wavy structure in the top of the Q, U, and PI images at about  $\ell = 163^\circ$  is caused by solar interference.

is still expanding freely into a low-density medium. In later stages, after the shock wave has been decelerated, the radio shell will look more compressed and will be better defined. The most likely explanation is the explosion of a massive object inside a stellar-wind bubble where the expanding shock wave has not yet reached the edge.

The large polarization bubble has a size of about  $9^\circ$  with about the same projected centre as the smaller one (see Fig. 2). The large bubble is only barely recognizable in the polarized intensity image and there is no counterpart in Stokes I, which makes this object a likely candidate for a Faraday Screen. However, there is no obvious counterpart visible in  $H\alpha$ , which indicates either a rather low electron density or a large distance. Since we see bright  $H\alpha$  emission from all three SNRs, all of which are located in the Perseus arm, the low electron density is the more likely explanation since a distance larger than the Perseus arm is highly improbable given the size of the bubble and the region of the Galaxy we are looking at. The spatial coincidence with the SNR VRO 42.05.01 indicates a Perseus arm location for the large bubble. The shape of VRO 42.05.01 implies that it is expanding into a quite homogeneous medium to the north and breaking out into a low density cavity in the south (Landecker et al., 1989). The breakout boundary of the SNR coincides exactly with the edge of this polarization bubble, strongly indicating an association. There is also an HI bubble coinciding with this large polarization structure (Fig. 2, lower right). A very large HI emission filament seems to surround the entire bubble structure as it is seen in Stokes Q and U. At the position of the SNR, this bubble contains bright sharp filaments with the same shape as the SNR, all of which have the same radial velocity of around  $-20$  km/s indicating a Perseus arm location about 1.5 to 2.0 kpc away from us. At this distance the polarization bubble has a length of 250 to 300 pc. The most likely explanation for the polarization characteristics is that this bubble contains a highly compressed magnetic field which leads to Faraday rotation of smooth Galactic background polarization coming from within the Perseus arm. It could be the remains of an old SNR, no longer visible in radio continuum, whose highly compressed magnetic field still affects the background emission.

It is not clear whether both polarization bubbles are related, but the SNR which creates the inner bubble must be expanding inside a low-density cavity. Since this SNR is located well inside the big bubble projected on the plane of the sky it is very likely that the SNR is indeed inside the old interstellar cavity that forms the large polarization bubble.

The region discussed was also observed with the Effelsberg 100-m telescope at the same frequency and an image including large-scale polarized emission exceeding 9'4 is shown by Reich et al. (this volume). It is planned to combine the CGPS and the EMLS for images being complete for all polarization structures larger than  $1'$ , which is the angular resolution of the CGPS.

## Acknowledgements

The Dominion Radio Astrophysical Observatory is a National Facility operated by the National Research Council. The Canadian Galactic Plane Survey is a Canadian project with international partners, and is supported by the Natural Sciences and Engineering Research Council (NSERC).

## References

- Brown J.C., Taylor A.R. (2001) *Astrophys. J., Lett.* **567**, L31  
 Landecker T. L., Pineault S., Routledge D., Vaneldik J. F. (1989) *Mon. Not. R. Astron. Soc.* **237**, 277  
 Taylor A.R., Gibson S.J., Peracaula M., et al. (2003) *Astron. J.* **125**, 3145.  
 Taylor J.H., Cordes J.M. (1993) *Astrophys. J.* **411**, 674.  
 Uyaniker B., Landecker T. L., Gray A. D., Kothes R. (2003) *Astrophys. J.* **585**, 785

# Polarization of the Outer Galaxy

Robert I. Reid

Dominion Radio Astrophysical Observatory, Herzberg Institute of Astrophysics, National Research Council of Canada, P.O. Box 248, Penticton, BC, Canada, V2A 6K3

**Abstract.** One of the products of the Canadian Galactic Plane Survey (CGPS) is a set of images of the outer Galaxy in Stokes Q and U at four frequencies clustered around 1420 MHz. These can be combined to form rotation measure maps, probing the magnetic field and free electron density of the warm ionized medium. Uyaniker, Landecker, Gray, and Kothes (2003) showed that because of spatially varying rotation measure the polarized emission of *extended* structures seen in the CGPS originates from within a "polarization horizon" roughly 2 kpc in radius in the direction of the local spiral arm.

This article discusses progress on an extension of the above work to a wider range in both longitude ( $l \in [75^\circ, 145^\circ]$ ) and latitude ( $b \in [-3^\circ, 19^\circ]$ ), to investigate the structure of the outer Galaxy's magnetoionic medium. Since extragalactic sources are generally unresolved and thus unaffected by the polarization horizon, comparing their rotation measures to that of diffuse emission in the same region in principle allows us to separate the Faraday rotation of the nearby Galaxy from that of the far outer Galaxy.

## 1 Introduction

The linear polarization of gigahertz radio waves is related to magnetic fields in two ways. Firstly, it is produced by synchrotron radiation from charges spiraling around magnetic fields, and the radiation is emitted with its plane of polarization perpendicular to the local magnetic field. Secondly, the plane of polarization is Faraday rotated by any plasma clouds along the line of sight that are themselves threaded by a magnetic field.

Specifically, the polarization angle  $\chi$  is rotated from its intrinsic value  $\chi_0$  according to

$$\chi = \chi_0 + \text{RM} \lambda^2 \quad (1)$$

$$\text{RM} = 0.81 \text{rad} \int \frac{n_e}{\text{cm}^{-3}} \frac{B_{\parallel}}{\mu\text{G}} \frac{dL}{\text{pc}} \quad (2)$$

RM is called the rotation measure and is proportional to the integral along the line of sight of the electron density multiplied by the component of the magnetic field parallel to the line of sight.

Equation 1 is exact for light from a single point source, but note that polarized emission can come from multiple places along the line of sight, with different RMs according to their distances. The received signal is the sum of the emission from all such components, and in general the polarization angle is *not* a linear function of the squared wavelength and the polarized intensity may change as well. The emission can also come from multiple directions within the telescope's beam, and the different directions may have different RMs, causing differential rotation and depolarization. Many ionized structures that create strong RM gradients, notably H II regions, can be detected as an absence of polarization surrounded by background polarized emission. Figure 3 shows a roughly N–S depolarization feature at  $l = 140^\circ 7'$ , corresponding to a filament visible in total intensity. On a larger scale, observations of linear polarization may exhibit a "polarization horizon" (PH) beyond which no polarized emission from *resolved* objects can be seen, due to an accumulation of depolarizers along the line of sight. The distance depends on the resolution, wavelength, and RM gradient in that direction. Point sources are unaffected by the PH, so the PH can be used to separate the foreground solar neighborhood from the outer reaches of the Milky Way, if the images have enough resolution to distinguish pointlike objects from extended ones.

## 2 Observations and Data Reduction

The Canadian Galactic Plane Survey (CGPS, Taylor et al. 2003) uses the Synthesis Telescope (ST) at the Dominion Radio Astrophysical Observatory to map with roughly  $1'$  resolution the portion of the galactic plane visible from southern British Columbia, along with a high latitude extension (Fig. 1). Polarization is measured in four continuum bands centered at 1406, 1414, 1427, and 1434 MHz, each with a bandwidth of 7.5 MHz.

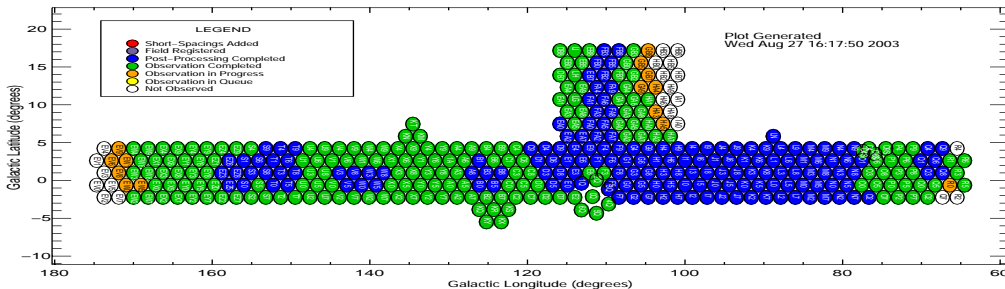


**Fig. 1.** Status of the CGPS polarization observations. The high latitude stripe is the blue stripe from  $b = 4^\circ$  to  $18^\circ$  at  $l = 111^\circ$ , and the high longitude regions discussed in this article are the blue islands at  $l = 125^\circ$  and  $143^\circ$ . The region from  $l = 82^\circ$  to  $95^\circ$  has already been discussed in Uyaniker et al. (2003) and the blue region at  $l = 154^\circ$  suffers from solar interference and is not included in this article.

The bands are close enough together that there is no “ $n\pi$ ” ambiguity in changes of polarization angle for  $|\text{RM}| < 3062 \text{ rad/m}^2$ . Sources with such large rotation measures on arcminute scales are rare and would tend to be depolarized in our survey, so they can be safely neglected.

Unfortunately the small angle differences between bands means that any interference and instrumental polarization must be carefully removed before measuring the RM of faint and/or diffuse emission. Thus the data used in this article is mainly limited by the region of the CGPS which has had its linear polarization processed.

Two perpendicular stripes were selected for processing and analysis. Each stripe is currently two fields wide, the minimum width that provides reasonably uniform coverage within the selected regions. The high latitude stripe is at  $l = 110^\circ$ , and extends from  $b = 2^\circ$  to  $b = 18^\circ$ . The high longitude stripe is really a string of three islands following the galactic midplane, at  $l = 116^\circ$ ,  $125^\circ$ , and  $141^\circ$ . There are higher longitude CGPS fields which have been processed in polarization, but they have not been included in this RM study because many of them were observed near solar maximum.

The unresolved sources (nearly all extragalactic) were separated from the broad scale (galactic) emission using a ring median filter (Secker 1995). The ring was a circular annulus with inner and outer diameters 1.5 and 3.0 FWHM beamwidths, respectively. Each pixel in the smooth image is the median value of the pixels in the annulus centered around the corresponding pixel in the original image. Subtracting the smooth image from the original image yields an image of the unresolved sources by themselves.

The rotation measures of the total linear polarization, median smoothed, and unresolved source images were calculated using a program by J. Brown (Brown et al. 2003). The program also produces an estimate of the uncertainty of each pixel’s RM.

The galactic RM,  $\text{RM}_g$ , was estimated in the midplane stripe as an average of pixels in slices one degree wide in longitude (or latitude, for the high latitude stripe), after rejecting any noise dominated pixels. The rejection was done at the break for each image in the histogram of pixel intensities between the noise distribution and the signal distribution. To minimize the error the averages were weighted by the inverse square of the uncertainty in each pixel:

$$\text{RM}_g = \frac{\sum_{\text{slice}} w \text{RM}}{\sum_{\text{slice}} w} \quad (3)$$

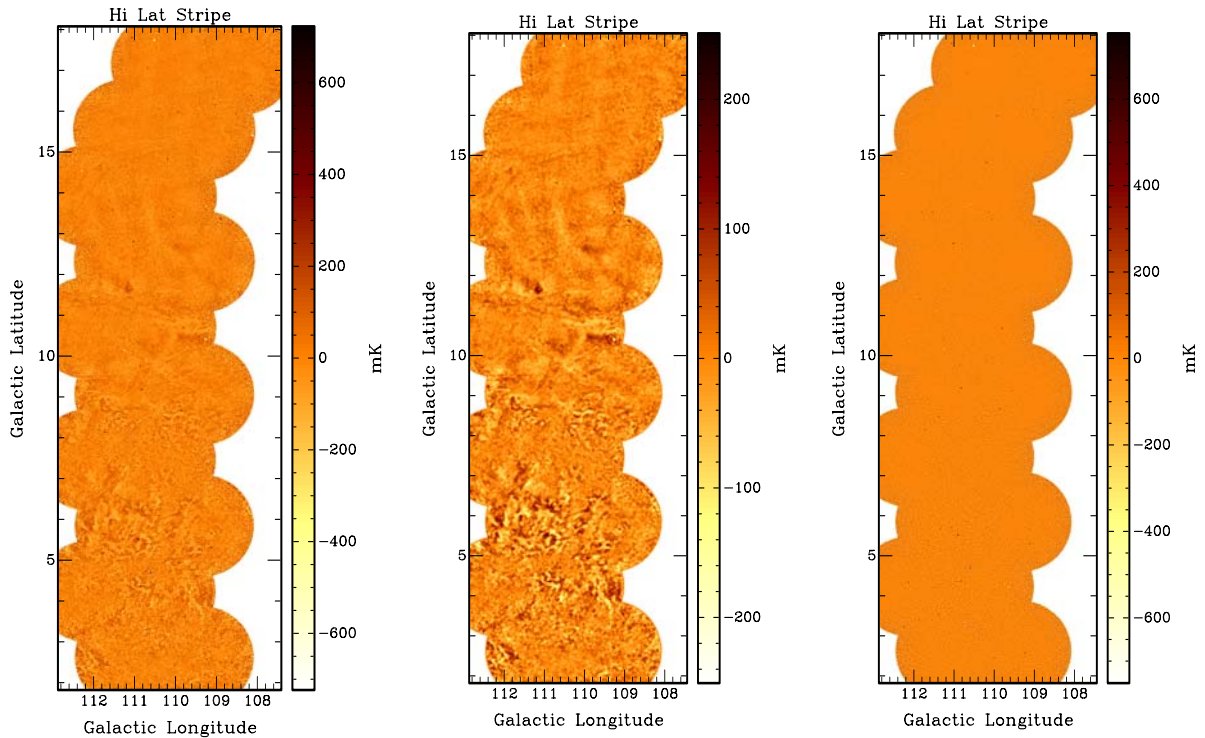


**Fig. 2.** The high latitude stripe in galactic Stokes U. Left: DRAO interferometer data from the CGPS. Middle: CGPS data median filtered using a circular ring with inner radius  $0'.75$  and outer radius  $1'.50$ . Right: CGPS data with the median filtered image subtracted, leaving the unresolved sources. All images are a combination of all four bands.

For the broad scale emission that uncertainty is simply the error in the slope of the  $\chi$  vs.  $\lambda^2$  relation, as calculated using the receiver noise. The unresolved sources have an additional contribution to the error of the galactic RM estimate, since they are mostly extragalactic and have intrinsic RMs. The extragalactic sources, and thus their intrinsic RMs, are independent and do not bias the average RM, but they do contribute shot noise. Taking the slope error to be unaffected by the intrinsic RM, the appropriate weight for unresolved sources is

$$w_{US} = (\sigma_{\text{slope}}^2 + \text{RM}_i^2)^{-1} \quad (4)$$

$|\text{RM}_i|$  cannot be calculated for each source without knowing the foreground  $\text{RM}_g$ , but the weights are only needed to minimize the variance of a nominally unbiased estimate, so it is sufficient to use a typical  $|\text{RM}_i|$  as measured from high latitude extragalactic objects.  $20 \text{ rad/m}^2$  was picked as a suitable value for this resolution and frequency.

The uncertainty of  $\text{RM}_g$  is

$$\sigma_{\text{RM}_g} = \frac{N^{1/2}}{b^{1/2} \sum_{\text{slice}} w} \quad (5)$$

where  $N$  is the number of pixels in the slice and  $b$  is the number of pixels in a beam area.

Brown et al. (2003) took care to exclude objects with noticeably nonlinear Faraday rotation or very high or low fractional polarization from their RM catalog of compact sources in the CGPS. Almost no inspection (as opposed to weighting) of individual sources has yet been made for this preliminary work. The exception is a source at G110.6+4.7, which is surrounded by obvious image artifacts. The pointing containing the W4 and W5 H II regions suffers from missing short baseline data, and was not included in this study. Also excluded, for now, were two pointings at  $l = 144^\circ$ , because of mild solar contamination.

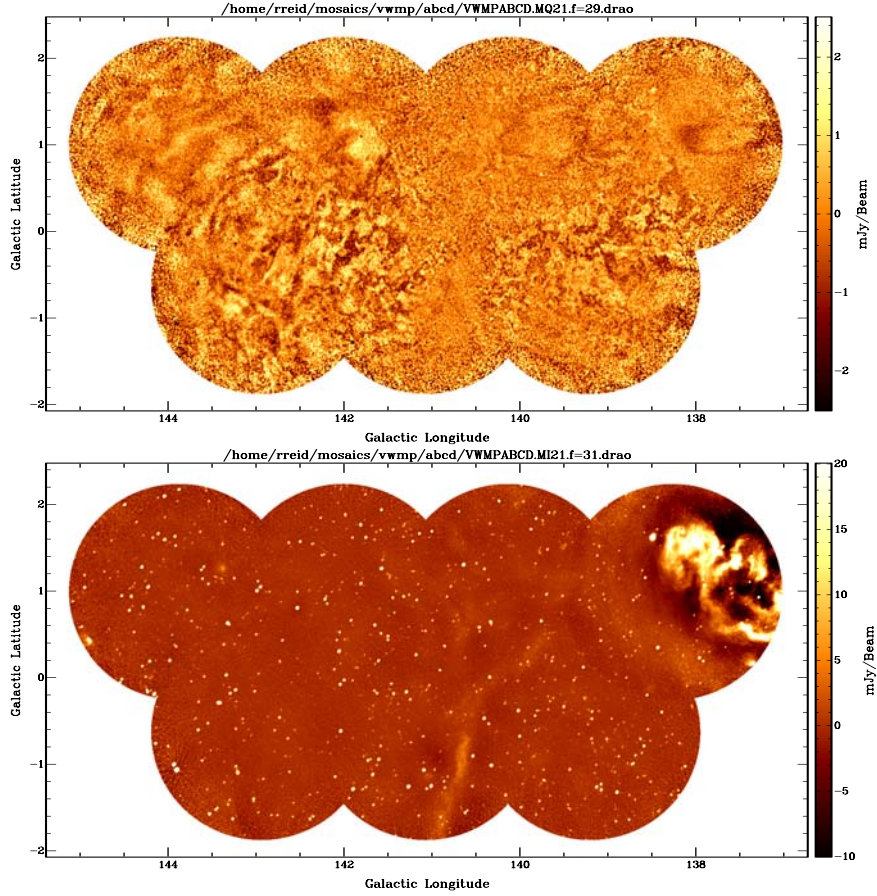


**Fig. 3.** The  $l = 141^\circ$  region in J2000 Stokes Q (top) and I (bottom), using data from all four bands.

### 3 Results and Interpretation

The longitudinal  $RM_g$  plots for total linear polarization and unresolved sources is on average consistent with the model in Brown & Taylor (2001) ( $RM_g = (-183 \pm 14) \cos(l - 84^\circ \pm 4^\circ) \text{rad/m}^2$ ), but exhibit some fairly large degree scale deviations. These regions feature several supernova remnants, an unusual smoothly polarized region, and a large depolarizing filament that could well be responsible. The  $200 \text{ rad/m}^2$  downturn in  $RM_g$  for the unresolved sources from  $l = 120^\circ$  to  $130^\circ$  is particularly interesting since it is echoed by a  $50 \text{ rad/m}^2$  downturn for structure within the PH. It may be that the region of extra RM is at the PH (and likely moving it closer in that direction), so that the resolved structure shows a decrease in RM due to the front part of the RM enhancement, while the light from the unresolved sources passes through the entire enhancement and shows the full effect.

The total polarization and unresolved sources panels of Fig. 6 show that  $|RM|_g$ , at least according to the unresolved sources, decreases with increasing latitude. The most serious fluctuations in the trend coincide with the positions of polarized filaments which are above and roughly parallel to the galactic disk (Fig. 2). The strong  $RM_g$  seen at the bottom of the high latitude stripe matches the expected value for  $RM_g$  within the disk at that longitude, and the total polarization and unresolved sources panels of Fig. 6 generally agree with the idea that  $RM_g$  is confined to a disk in the galactic plane, since that is where certainly the electron density and possibly the magnetic field are strongest.

The relative strengths of the average RMs for the resolved and unresolved sources indicates that  $|RM|$  increases with distance, and does not show any evidence for a reversal of the magnetic field in the outer Galaxy, at least at these longitudes. The distance to the CGPS PH has previously been estimated to be on the order of one or two kiloparsecs in the disk (Uyaniker et al. 2003), so the higher latitude

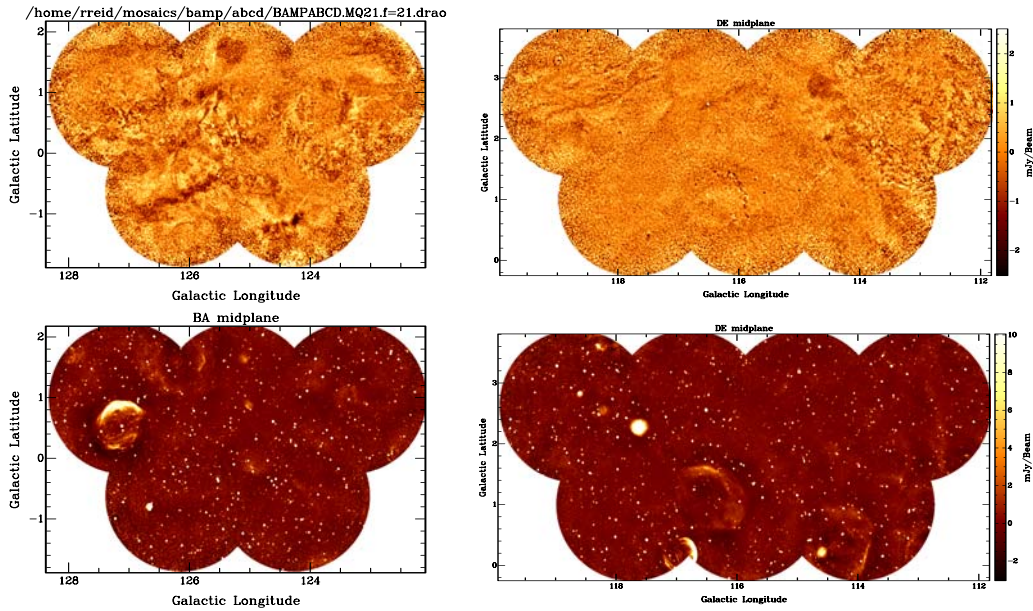


**Fig. 4.** The  $l = 116^\circ$  and  $125^\circ$  regions in J2000 Stokes Q (top) and I (bottom), using data from all four bands.

lines of sight should be “breaking free” of disk depolarization even for resolved objects. Figure 2 shows a change (i.e. disappearance) as expected in polarization structure, but the resolved RM (right panel of Fig. 6) is quite constant. The average extragalactic  $RM_g$  appears to match the average resolved RM at the high latitude limit of the measurements, so it may be that there is no change in RM to see. In other words, it could be that the high latitude lines of sight are unobstructed, but that the  $RM_g$  there happens to match the resolved RM for lower latitudes. Unfortunately there is not enough signal in the high latitude stripe to measure the resolved RM for  $b > 12^\circ$ .

The resolved RM has two other possible problems. After the rejection of pixels below the threshold signal strength, the remaining pixels in the median filtered images tend to consist of one or two connected regions per degree of longitude or latitude. This means that currently the average resolved RM could say more about individual objects than the Galaxy as a whole, although the fluctuations appear to be small. Also, the ST is an interferometer, and misses flux from very smooth ( $\gtrsim 45'$ ) structures, which can distort the measured RMs, even of sharper features superimposed on the smooth structures. It is known (W. Reich, private communication 2003) that there is significant smooth polarized structure at least in the high latitude stripe, casting the ST extended emission RMs into doubt, especially since they are much larger than the RMs measured in that region by Brouw and Spoelstra (Brouw & Spoelstra 1976, Spoelstra 1984) using a single dish antenna at Dwingeloo. On the other hand, the ST extended emission RMs are concordant with the unresolved RMs of this paper, and a general trend of observing larger RMs when a smaller beam is used. Since we have good reason to believe that smoother features tend to be closer, it is likely that the Dwingeloo RMs are smaller because most of the observed polarized emission has travelled a shorter distance through the ISM. They may also be affected by the changing beam size between the lowest (408 MHz) and highest (1411 MHz) frequencies. Ideally the RMs of objects from a few arcminutes to a few degrees in extent should be determined using a combination of single dish data (to capture all of the flux) and interferometer data (to eliminate confusion), but in practice combining existing datasets is nontrivial.

Fortunately the median filtering protects the unresolved source RMs from any effects of missing broad scale flux. Since any object in the CGPS larger than  $10'$  is galactic, there is enough room to median filter the already median filtered images at a medium scale to measure RMs of objects within the PH. Widening this study to the entire CGPS (Fig. 1) should provide a large enough sample to ameliorate the above two problems.

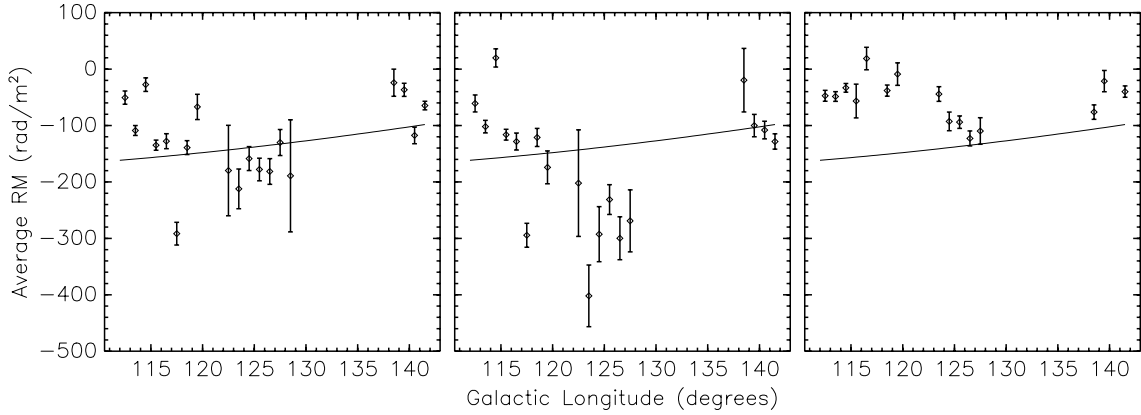


**Fig. 5.** Longitudinal dependence of RM. Left: RM of total linear polarization as seen by the ST. Middle: RM of unresolved sources. Right: RM of resolved structures. The error bars represent one standard deviation. The curve is the galactic RM model of Brown & Taylor (2001).

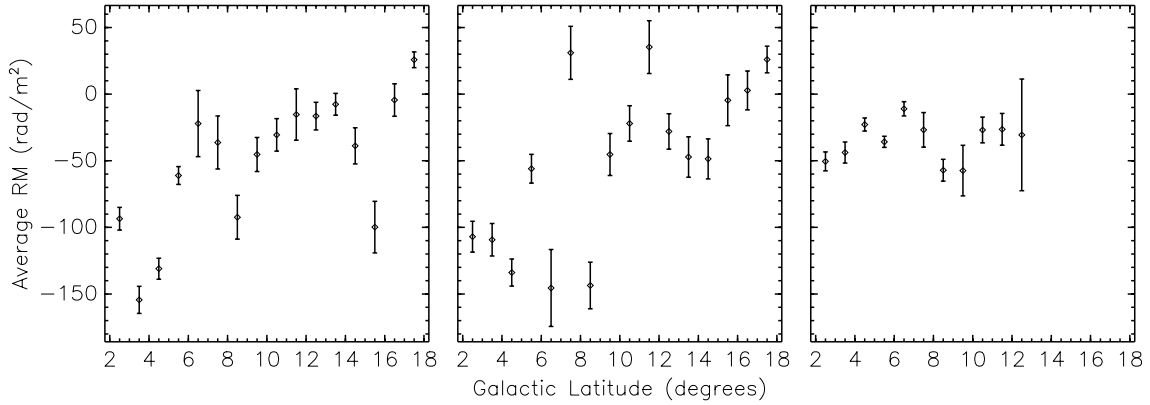


**Fig. 6.** RMs of the high latitude stripe. Left: RM of total linear polarization as seen by the ST. Middle: RM of unresolved sources (rightmost image of Fig. 2). Right: RM of median filtered (smooth) structures (middle image of Fig. 2). The error bars represent one standard deviation.

## Acknowledgments

This article has greatly benefited from comments by T. Landecker and W. Reich, and I thank R. Kothes, T. Foster, and P. Kronberg for their helpful conversations. J. Brown graciously provided her RM calculation program and a brief introduction to IDL. C. Brunt, S. Dougherty, and R. Kothes processed the Stokes I data used to correct the Q and U data, and some of the polarization data was processed by B. Uyaniker. The Canadian Galactic Plane Survey is a Canadian project with international partners and is supported by the Natural Sciences and Engineering Research Council of Canada (NRC). The Dominion Radio Astrophysical Observatory is operated as a National Facility by NRC.

## References

- Brouw, W., Spoelstra, T. (1976) *Astron. Astrophys. Suppl.* **26**, 129.  
 Brown J.C., Taylor A.R. (2001) *Astrophys. J., Lett.* **563**, 31.  
 Brown J.C., Taylor A.R., Jackel, B.J. (2003) *Astrophys. J. Suppl.* **145**, 213.  
 Secker J. (1995) *Publ. Astron. Soc. Pac.* **107**, 496.  
 Spoelstra, T. (1984) *Astron. Astrophys.* **135**, 238.  
 Taylor A.R., Gibson S.J., Peracaula M., Martin P.G., Landecker T.L. et al. (2003) *Astron. J.* **125**, 3145.  
 Uyaniker B., Landecker T.L., Gray A.D., Kothes R., (2003) *Astrophys. J.* **585**, 785

# The Effelsberg 1.4 GHz Medium Galactic Latitude Survey (EMLS)\*

W. Reich, E. Fürst, P. Reich, B. Uyaniker, R. Wielebinski and M. Wolleben

Max-Planck-Institut für Radioastronomie, Auf dem Hügel 69, 53121 Bonn, Germany

**Abstract.** We describe a recently completed 1.4 GHz continuum and polarization survey carried out with the Effelsberg 100-m telescope. The survey covers the northern Galactic plane in the latitude range of  $\pm 20^\circ$ . The most spectacular results are from the polarization maps, which show an unexpected richness in structure with almost no counterpart in total intensity. Variations in the Faraday rotation properties within the nearby magneto-ionic interstellar medium are largely responsible for the observed structures. Numerous Faraday screens are indicated in the maps. However, absolute calibration is quite essential for the interpretation of polarized structures. This needs additional data. We give an outline of the EMLS properties and demonstrate its potential to understand the properties of the interstellar medium.

## 1 Introduction

The intensity of Galactic synchrotron emission observed from a certain direction depends on the strength of the Galactic magnetic field and its orientation. Its regularity is reflected by the amount of percentage polarization. However, the superposition of emission regions with different magnetic field orientations and in addition Faraday rotation effects along the line of sight result in complex structured polarization images, which are not straightforward to interpret (see e.g. Uyaniker, this volume). Faraday rotation decreases with  $\nu^2$ , so that high-frequency observations are preferable for a study of the intrinsic Galactic magnetic field properties. However, the weak signals at high frequencies require high sensitivities and until recently no large-scale polarization measurements with sufficient angular resolution could be made. Here we describe a 1.4 GHz Galactic plane survey project reaching medium Galactic latitudes, which should serve as the basic data set for global as well as detailed studies of magnetic fields and the magneto-ionic medium.

## 2 Observations

The Effelsberg 100-m telescope has an L-band receiver with a frequency range from 1.29 GHz up to 1.72 GHz installed in its primary focus. Sensitive continuum and polarization observations at L-band with a sufficiently wide bandwidth are difficult to perform because of numerous sources of interference. Therefore we placed the centre frequency close to the protected band at 1.4 GHz, but excluding Galactic H I emission. During most of the observing time we could use 20 MHz or at least 10 MHz bandwidth. The angular resolution of the telescope is  $9/35$  at 1.4 GHz. The receiver has two channels with cooled HEMT amplifiers for the LHC and the RHC components from a single feed. An IF-correlation polarimeter provides two total intensity channels, e.g. the LHC and RHC channel assuming no circular polarization, and two correlated channels proportional to Stokes U and Q (see Uyaniker et al., 1998).

The Effelsberg telescope was used to map a large area of the northern Galactic plane (EMLS) as shown in Fig. 1. The area was split in subfields of typically  $10^\circ \times 10^\circ$  with  $5^\circ$  as the smallest and  $16^\circ$  as the largest scan length. Each field in Galactic coordinates was observed twice in orthogonal scanning directions. The total integration time per  $4' \times 4'$  pixel is 2 sec, which is sufficient to reach

---

\*Based on observations with the Effelsberg 100-m telescope operated by the Max-Planck-Institut für Radioastronomie (MPIfR), Bonn, Germany

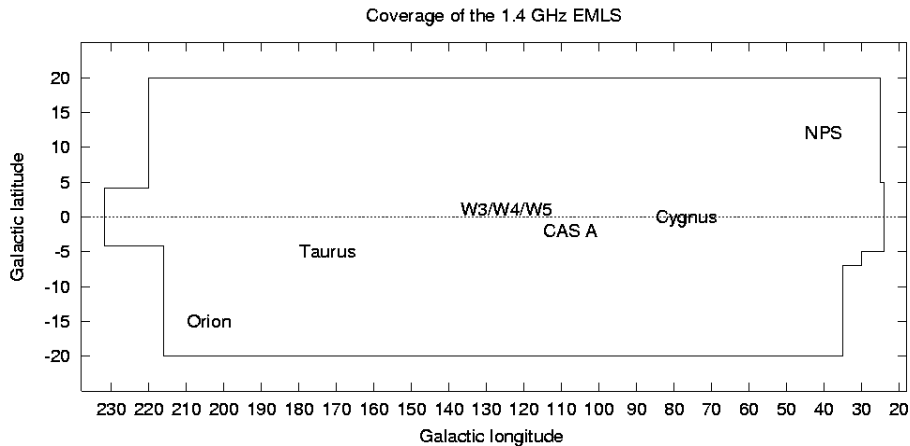


Fig. 1. Area covered by the EMLS. A number of prominent source complexes are indicated.

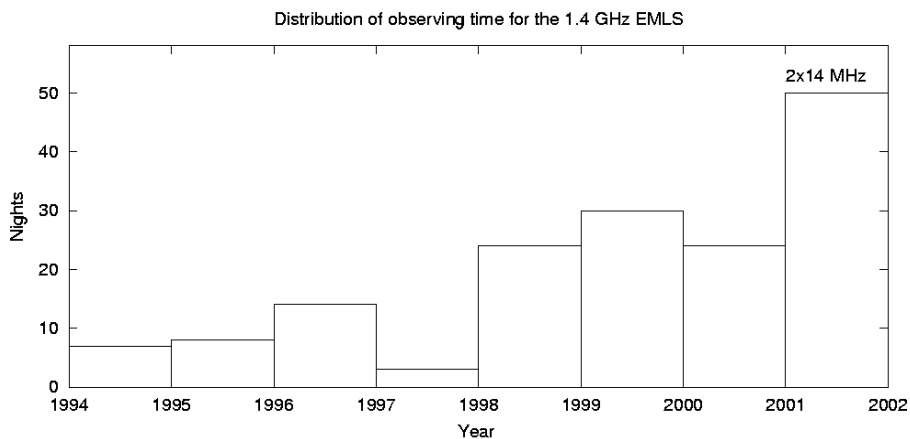


Fig. 2. Statistics of observations. In total about 1000h of net-observing time was allocated for the survey observations.

the confusion limit of about 7 mJy/beam-area or 15 mK rms-noise in total intensity. Measurements of polarized emission are not limited by confusion. The rms-sensitivity is about 8 mK in U and Q.

The observations were spread over a period from 1994 to 2002 (Fig. 2). Since the Effelsberg telescope operates up to mm-wavelengths high-frequency observations have priority and large projects in the decimeter ranges are delayed. In addition, the L-band observations suffer from interference, which sometimes forced interruptions up to several months.

We used a single IF-polarimeter for all observations carried out until the end of 2001. Later two polarimeters with 14 MHz bandwidth each were used simultaneously at central frequencies of 1395 MHz and 1408 MHz. A few measurements with distortions identified in the data reduction process were repeated recently using a new 8-channel polarimeter centered at 1402 MHz with a total bandwidth of 32 MHz.

### 3 Reduction and absolute calibration

The principles of data reduction and absolute calibration were already described in some detail by Uyaniker et al. (1998). The total intensity and polarization data were edited and calibrated using standard procedures for Effelsberg observations. Specific care must be taken for L-band polarization data because a significant cross-talk from the broad-band polarization transducer (OMT) of the receiver is present. However, correcting for this effect reduces the residual instrumental polarization to

less than 1%. The maps were scaled by comparison with standard calibration sources, where 3C286 with well-defined polarization properties served as the primary calibrator. The final maps are stored in main beam brightness temperatures ( $T_b/S = 2.12 \text{ K/Jy}$ ).

Baseline setting at the boundaries of the individual fields observed is a necessity to get data free from system noise, atmospheric and ground radiation contributions. These temperature offsets depend on elevation and may also vary with time. The process of baseline setting, however, also subtracts large-scale emission from the data with scales from about the size of the observed field and larger. We recovered these components by comparing the data with absolutely calibrated low-resolution surveys at the same frequency and added the missing structures. The total intensity data were corrected by the absolutely calibrated 1.4 GHz Stockert survey with  $36'$  angular resolution (Reich, 1982; Reich & Reich, 1986). The correction for polarization data turned out to be more difficult. We had access to a polarization survey of the northern sky at 1411 MHz by Brouw & Spoelstra (1976). However, this survey is largely undersampled, of limited sensitivity and does not cover the entire area of the EMLS. An absolute calibration of polarized emission is, however, essential. Missing large-scale structures in Stokes U and Q will completely change the resulting polarized intensity ( $PI = (U^2 + Q^2)^{0.5}$ ) structures and also the distribution of polarization angles PA. The non-linear dependence of U and Q on PI and the dependence on the relative signs of large and small-scale emission in U and Q have large effects. Small-scale PI structures seen as emission maxima may turn into structures with minima compared to their surroundings in an absolutely calibrated PI map. Minimum structures (for example the often discussed ‘canals’) may completely disappear after absolute calibration. Any interpretation of polarized emission must take such effects into account carefully. On the other hand, there is clearly a need to improve the available absolutely calibrated polarization data observed more than 30 years ago (Reich & Wielebinski, 2001). For that purpose scans at fixed declinations were observed using the DRAO 26-m telescope equipped with an Effelsberg IF-polarimeter of the same type as used for the EMLS. These data will provide the missing information in the EMLS. This survey was carried out in 2001/2002 and is described by Wolleben et al. (this volume) and will serve as the basis for the EMLS absolute polarization calibration.

## 4 Example maps

First maps from the survey in different Galactic directions were already published by Uyaniker et al. (1999). However, as noted above the polarization maps have to be taken as preliminary because of limited absolute calibration available at that time. The first survey maps published are accessible from the MPIfR survey sampler in FITS-format via <http://www.mpifr-bonn.mpg.de/survey.html>. Also other continuum surveys are accessible from that address.

Here we show as another example of an EMLS map a large section of the Galactic plane towards the Galactic anticentre direction. Figure 3 displays absolutely calibrated total intensity and (preliminary) polarization intensity maps, but for comparison also ‘relative’ polarized intensities as observed directly with the Effelsberg telescope. Unfortunately, the absolute polarization map is limited due to insufficient Dwingeloo data for this field, in particular for negative Galactic latitudes where the Effelsberg polarization maps show strongest emission. From the average U and Q values in the field we noted a gradient from negative to positive Galactic latitudes and applied the following linear corrections to the Effelsberg U, Q maps: 140 mK/320 mK at  $+4^\circ$  and 0 mK/280 mK at  $-4^\circ$  Galactic latitude. This is definitely a simplification of the real large-scale polarized background, but the magnitude of correction is in the right range. The large Q value added reflects the presence of a homogeneous large-scale field running almost parallel to the Galactic plane. The mean polarized intensities increase after absolute calibration from 123 mK to 347 mK. While the shape of the intensity distributions of the U and Q maps remains unchanged, the dispersion of PI increases slightly from 83 mK to 91 mK. The distribution of absolute and relative PIs (Fig. 4) shows large differences in their mean levels, but in particular in the shape of the intensity distributions.

A number of discrete large-diameter objects can be easily distinguished from the general diffuse emission in the area of Fig. 3. There are supernova remnants (G160.0+2.6(HB9), G166.0+4.3(VRO 42.05.01) or G166.2+2.5(OA184)) as well as H II region complexes (Sharpless regions SH229–237)

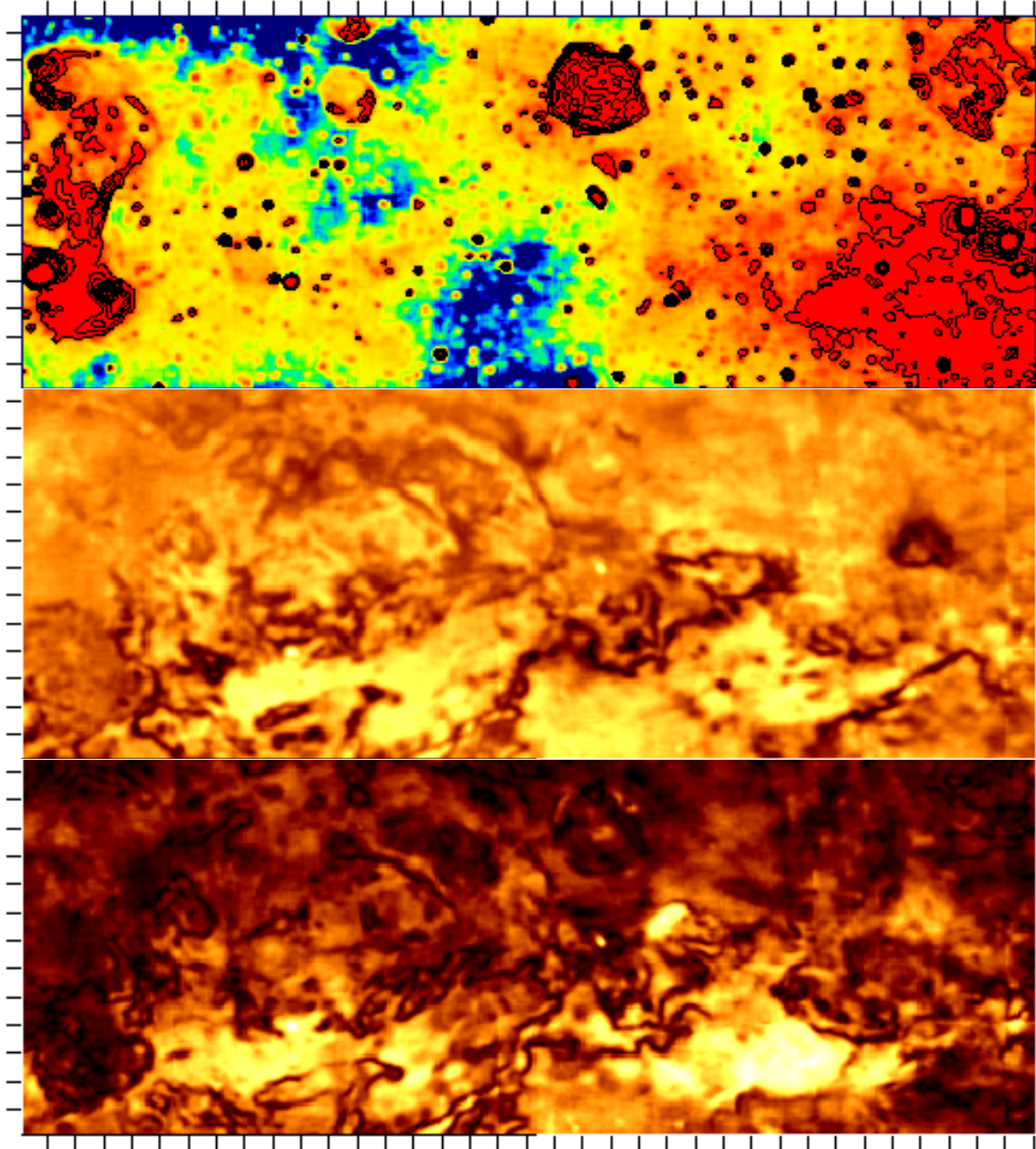


**Fig. 3.** A  $24^\circ \times 9^\circ$  section of the 1.4 GHz EMLS centered at  $l, b = 162^\circ, 0^\circ$ . Absolutely calibrated total intensities are shown on top with color-coded intensities running from 4.5 K to 5 K. Contours are shown for intensities above 5 K in steps of 0.25 K  $T_b$ . Polarized intensities with preliminary absolute calibration are displayed from 0 mK to 850 mK (middle). The Effelsberg data with missing large-scale structures are shown for comparison (bottom). Polarized intensities run from 0 mK to 500 mK.

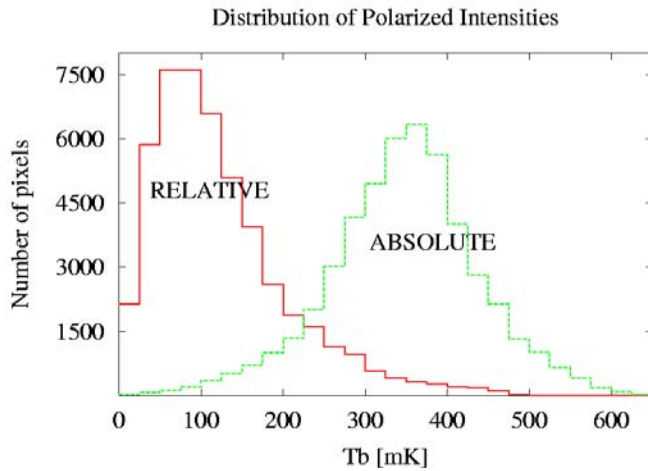


**Fig. 4.** Modification of the polarized intensity distribution by absolute calibration for the data shown in Fig. 3. ‘Relative’ means Effelsberg data only.

around  $l = 173^\circ$ . The diffuse emission is quite patchy and the pronounced ridge from the thin disk of the Milky Way as seen from the inner Galaxy is not evident in this direction. PIs distribute rather different when compared to total intensities. This reflects large-scale variations in Faraday rotation effects along the line of sight.

When comparing the two polarization maps shown in Fig. 3 clear differences are evident: The shape and distribution of small-scale structures is different, some features turn from emission structures in the Effelsberg map into polarization minima after absolute calibration. For instance the planetary nebula PK158+00(S 216) at  $l, b = 158^\circ, 0^\circ$  with a diameter of about  $1.6'$  almost disappears in the absolutely calibrated map. PK158+00 is at a distance of about 120 pc and acts as a Faraday screen (Uyaniker, this volume). Other local Faraday screens towards a Taurus molecular cloud are discussed by Wolleben & Reich (this volume). Faraday screens affect all polarized emission from behind and thus local features have a larger effect on polarization maps than more distant ones, which also appear smaller in size. The origin of Faraday screens in the interstellar medium, which require a large regular magnetic field strength and/or a high thermal electron density, remains to be investigated.

Another example of a quite large coherent polarization feature, which very likely indicates the presence of a Faraday screen in the solar vicinity, is shown in Fig. 5. This elliptically shaped structure has a size of about  $\sim 8^\circ$  along its major axis. Although this feature has not been investigated in detail yet, it reflects the properties of a passive Faraday screen rotating the background polarization in a sense that (from outside to inside) a ring of enhanced intensities is visible followed by a polarization minimum and apparently unchanged intensity in the centre. This behaviour suggests that background polarized emission is successively rotated and adds with unchanged foreground emission in a way that vectors get more aligned (maximum) and then less aligned (minimum), while towards the centre a rotation close to  $\pi$  is suggested. In the EMLS maps we see numerous features resembling Faraday screens. Missing distance information is a problem when deriving their spatial density. Faraday screens complicate the modelling of observations. They cannot be described by polarization transfer models assuming a turbulent interstellar medium nor by models assuming a mixture of Faraday rotating material with synchrotron emission only. Also rotation measures towards Faraday screens vary as they depend on the wavelengths of measurements (Wolleben & Reich, 2004). This means that polarization angle variations do not follow a  $\lambda^2$  dependence.

## 5 Outlook

The EMLS will be the basis for more detailed polarization studies by following up specific structures at higher frequencies or repeating observations with the now available multi-channel polarimeter for rotation measure determinations. Another important project is the combination of the EMLS with the DRAO 1.4 GHz survey of the Galactic Plane (CGPS), which has about  $1'$  angular resolution.

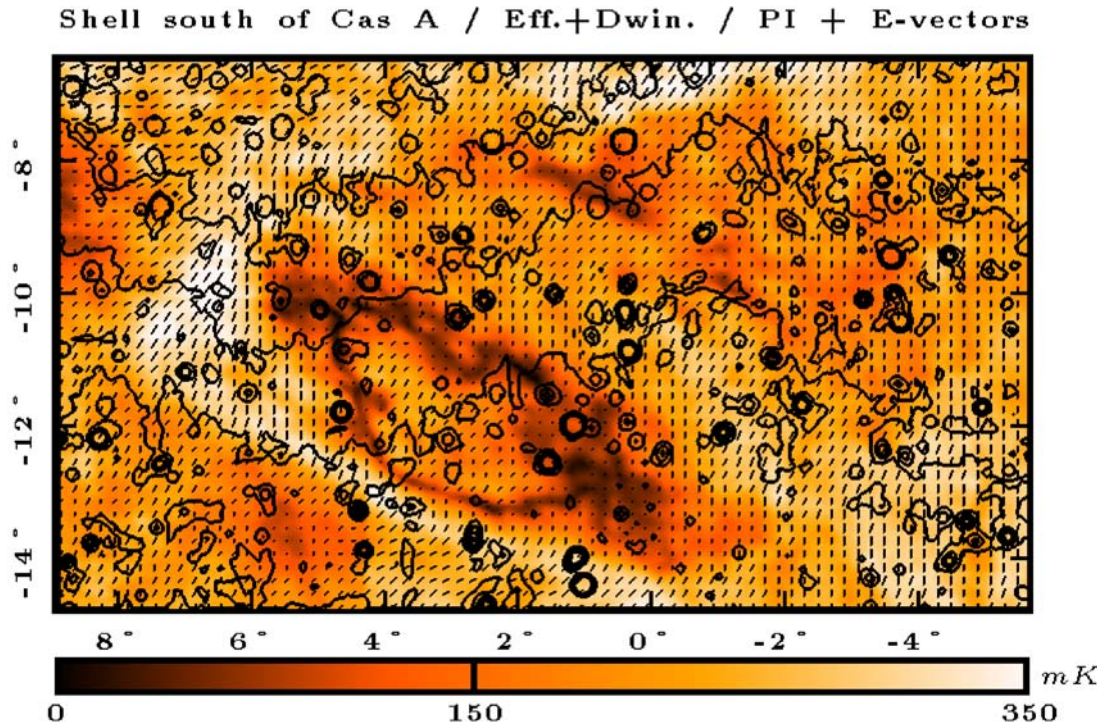


**Fig. 5.** A section of the 1.4 GHz EMLS showing a large polarized shell structure. Galactic longitudes are relative to  $l12^{\circ}5$ , while latitudes are absolute. Overlaid are contours of total intensities, which do not indicate any emission corresponding to the polarization structure. The large majority of the numerous compact sources is extragalactic.

Example maps from the region shown in Fig. 3 are included in the contribution by Kothes & Landecker (this volume), where the higher angular resolution not only uncovers small-scale structures, but also significantly reduces the effect of beam depolarization.

A polarization survey at a single frequency is just the starting point of further measurements to obtain rotation measures, which reflect the physical properties of the interstellar medium. Narrow-band polarimetry, as carried out at DRAO (Kothes & Landecker; Reid, this volume), at Westerbork (Haverkorn et al., this volume and references therein) or ATCA (Gaensler et al., 2001) are one possibility, which is now also available at the Effelsberg telescope. Nonlinear effects and a precise determination of polarization angles require a wider frequency range. High-frequency observations of large EMLS sections are needed and planned for  $\lambda 6$  cm using the Urumqi telescope (China). Large-scale high-frequency work is also urgently required for a better estimate of the influence of Galactic foreground polarization on high-frequency cosmic microwave background polarization measurements. Beside of future observational efforts also more complex modelling is required to understand polarization observations and the properties of the interstellar medium.

## References

- Brouw W. N., Spoelstra T. A. Th. (1976) *Astron. Astrophys. Suppl.* **26**, 129.  
 Gaensler B. M., Dickey J. M., McClure-Griffiths N. M. et al. (2001) *Astrophys. J.* **549**, 959.  
 Reich P., Reich W. (1986) *Astron. Astrophys. Suppl.* **63**, 205.  
 Reich W. (1982) *Astron. Astrophys. Suppl.* **48**, 219.  
 Reich W., Wielebinski R. (2001) in *Radio Polarization: a New Probe of the Galaxy*, ed. T. L. Landecker, Université de Montreal, p. 55.  
 Uyaniker B., Fürst E., Reich W., Reich P., Wielebinski R. (1998) *Astron. Astrophys. Suppl.* **132**, 401.  
 Uyaniker B., Fürst E., Reich W., Reich P., Wielebinski R. (1999) *Astron. Astrophys. Suppl.* **138**, 31.  
 Wolleben M., Reich W. (2004) *Astron. Astrophys.*, submitted.

## The DRAO 26-m Large Scale Polarization Survey at 1.41 GHz

M. Wolleben<sup>1,2</sup>, T.L. Landecker<sup>2</sup>, W. Reich<sup>1</sup> and R. Wielebinski<sup>1</sup>

<sup>1</sup>Max-Planck-Institut für Radioastronomie, Auf dem Hügel 69, 53121 Bonn, Germany

<sup>2</sup>Dominion Radio Astrophysical Observatory, Herzberg Institute of Astrophysics, National Research Council of Canada, Box 248, Penticton, BC V2A 6J9, Canada

**Abstract.** The Effelsberg telescope as well as the DRAO synthesis telescope are currently surveying the Galactic polarized emission at  $\lambda 21$  cm in detail. These new surveys reveal an unexpected richness of small-scale structures in the polarized sky. However, observations made with synthesis or single-dish telescopes are not on absolute intensity scales and therefore lack information about the large-scale distribution of polarized emission to a different degree. Until now, absolutely calibrated polarization data from the Leiden/Dwingeloo polarization surveys are used to recover the missing spatial information. However, these surveys cannot meet the requirements of the recent survey projects regarding sampling and noise and new polarization observation were initiated to complement the Leiden/Dwingeloo Survey. In this paper we will outline the observation and report on the progress for a new polarization survey of the northern sky with the 26-m telescope of the DRAO.

### 1 Motivation

Over the past several years a number of survey projects were launched in order to map the polarized emission from the Galaxy in great detail (e.g. Junkes et al. 1987, Duncan et al. 1997, Uyaniker et al. 1998, Taylor et al. 2003). Single-dish as well as synthesis telescopes located in the northern and southern hemisphere are being used. However, observations made with synthesis telescopes are systematically affected by a missing zero spacing problem, which prevents the detection of extended emission. In a similar way, single-dish observations can lack a large-scale emission component, which is often lost during the data reduction process when attempts are made to subtract the ground radiation from the observations. If the ground radiation is not known exactly, one cannot distinguish between real sky signal and radiation from the ground.

For an interpretation of polarimetric observations, an accurate absolute calibration is essential. Other than for total power observations, absolute calibration of polarization data means to calibrate vectorial quantities. Surprisingly on first sight, this means that absolute calibration of polarized intensity maps can turn emission-type objects into minima in PI, and vice versa. Also rotation measures can be affected by an inaccurate calibration of polarization data.

Missing zero spacings in interferometric observations are added from single-dish observations. In turn, large-scale components in single-dish data are recovered by using existing absolutely calibrated polarization data from the 60's and 70's made with single-dish telescopes, e.g. the Leiden/Dwingeloo polarization surveys (Brouw & Spoelstra 1976). However, the severe under-sampling and relatively high noise of these data often makes an accurate calibration of the recent surveys impossible. Until now, these absolutely calibrated data from the Leiden/Dwingeloo surveys laid the foundation for the calibration chain up to the synthesis telescopes, and therefore an improvement of these *old* data regarding sampling and noise became necessary.

### 2 The DRAO 26-m Telescope and Receiver

The 26-m telescope at DRAO is on an equatorial mount, with a mesh surface and the receiver placed in its prime focus on three feed-legs. The pointing accuracy is about  $48''$ . The receiver used for polarimetric observations consists of a quadrature HF-hybrid which forms circular out of linear polarization,

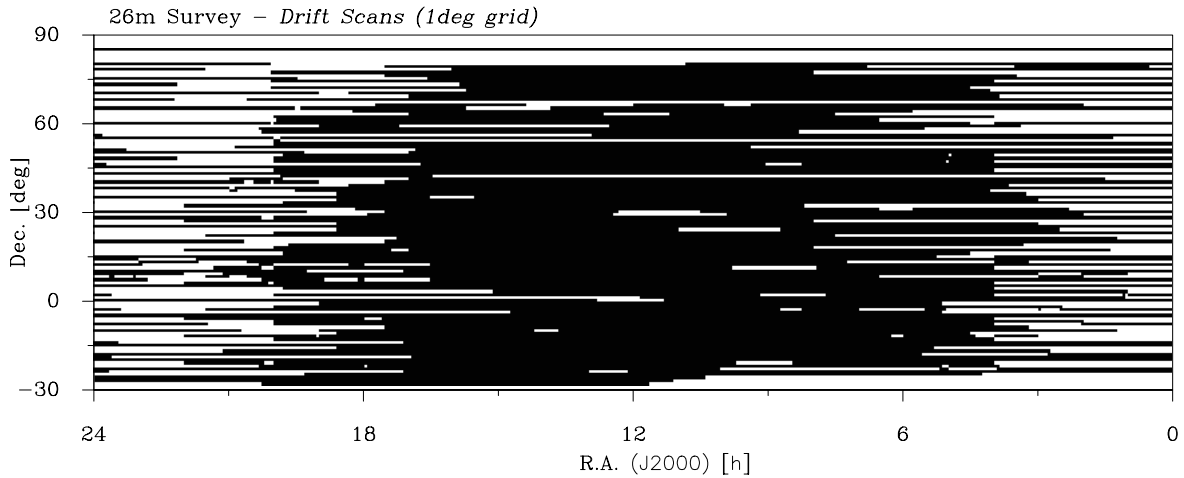


**Fig. 1.** Map showing the sky coverage of the new survey. Black lines indicate drift scans.

two uncooled FET-amplifiers for both hands of polarization operating on room temperature, and circulators to improve matching. The system temperature was about 150 K. Two HF-bandpass filters and additional IF-filters were used to limit the bandwidth to 12 MHz (10 MHz for data obtained in November 2002). An integrated noise source was used to inject a calibration signal every 32 seconds for a duration of 400 ms into the X and Y part of the receiving system. Gain variations were less than 4% over a period of 40 days.

The IF-polarimeter is an analog 2-channel multiplier providing the four correlation products RR, LL, RL, and LR. The polarimeter was brought from the MPIfR, Bonn and is of the type used on the Effelsberg telescope. It operates at an IF of 150 MHz and a total bandwidth of 50 MHz. Every 4 seconds, an internal phase shifter was switched to invert the signs of the two cross-correlation products. This was necessary to correct for any electronic drifts in the polarimeter. Data were integrated and recorded every 40 ms.

### 3 Observation, Calibration and Reduction Steps

Observations were made during seven months from November 2002 through May 2003 using the 26-m telescope in the drift-scan mode. Each night one declination was observed. We made 168 drift scans covering the entire sky observable from the DRAO with the telescope stationary on the meridian. Many regions could be observed with a  $1^\circ$  separation in declination or smaller; some could only be observed with a  $5^\circ$  sampling in declination. Along right ascension the drift scans are fully sampled. The center frequency of the receiver was tuned to 1410 MHz, avoiding the H I line emission. Most of the observations were done during the night. Prior and after each drift scan, standard calibration sources were mapped.

The hybrid introduces cross-talk and extensive calibration was needed to transform the four polarimeter output channels into true Stokes parameters. The following steps were applied to the raw data:

**Flagging:** Interference removal was done automatically by a flagging algorithm which searches for short-term peaks which are  $4.5 \sigma_{\text{rms}}$  above the average signal level over a 2 minute time window.

**Pre-scaling and rotation:** The vector formed out of the four correlation products RR, LL, RL, and LR is multiplied with a  $4 \times 4$ -matrix, similar to a Müller matrix with the difference that correlation products instead of Stokes parameters are transformed. This reduction step includes a pre-scaling and rotation in order to transform the arbitrary polarimeter units into meaningful temperatures in the equatorial system. An iterative method is used to find the appropriate

correction matrix. This algorithm starts with the unit matrix and successively modifies matrix entries until the best-fit matrix is found. The quality of the matrix can be estimated by the correlation of the corrected raw data with the absolutely calibrated Leiden/Dwingeloo polarization data, resp. the Stockert total-power data (Reich 1982, Reich & Reich 1986).

**Gain and phase:** Electronic gain and phase variations in the receiving system were recorded by changes in the signal level of the calibration signal in all four channels. The standard temperature and position angle of the calibration signal assumed for this survey is given by the average values over the seven months.

**Ground radiation:** Spurious polarization is picked up by the side-lobes of the telescope. This mainly ground-based signal can be intrinsically unpolarized, however, the side-lobes are highly polarized, which results in an elevation- and azimuth-dependent polarization component. Since we exclusively observed in the meridian we only have to deal with the elevation dependency. For the purpose of deriving a ground-radiation model we made elevation scans along the meridian at different sidereal times. Their average served as a time-independent model (see Fig. 2) which was used to subtract the ground-radiation component.

**Sun and ionospheric Faraday rotation:** Beside the rather stable ground radiation, which was modelled, the sun is another strong source of spurious polarization. In the same way as the ground is detected as a polarized signal, the bright signal from the sun also causes strong polarized signals if radiating into the side-lobes. Therefore observations were limited to night-time to circumvent interference from the sun. In addition, ionospheric Faraday rotation can affect the position angle of polarized signals. This effect is negligible during the night. Whenever day-time data were used, we cross-checked the data against neighboring drift scans for possible sun interference or ionospheric Faraday rotation.

**De-stripping:** Although the receiving system is fairly stable, there are remaining variations in the system temperature. We believe that these variations are caused by seasonal changes of the ground radiation or temperature drifts in the front-end part of the receiver. Changing offsets in the system temperature show up as stripes in the final map and we compared in an iterative method each drift scan with its neighboring scans to correct for variations in the system temperature.

**Final scaling, rotation, and instrumental polarization:** After applying the reduction steps discussed above, a second pass Müller matrix fit was necessary to improve the correlation with the reference values from the Leiden/Dwingeloo survey. Also the cross-talk introduced by the receiver was now corrected.

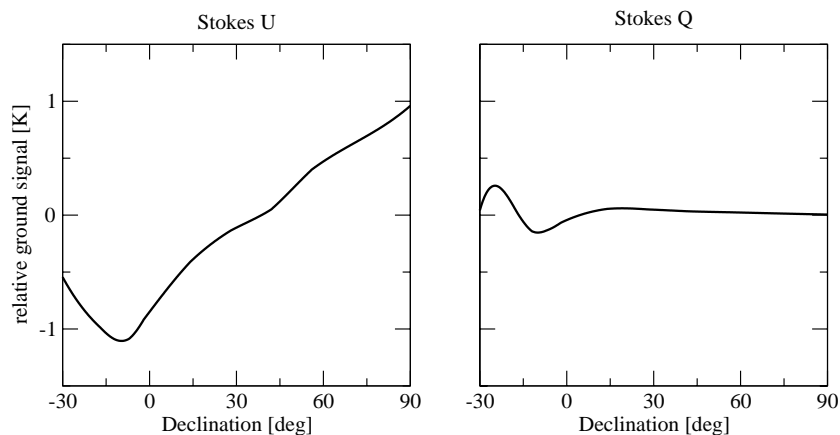


**Fig. 2.** Ground radiation profiles for Stokes  $U$  and  $Q$  derived by averaging elevation scans.

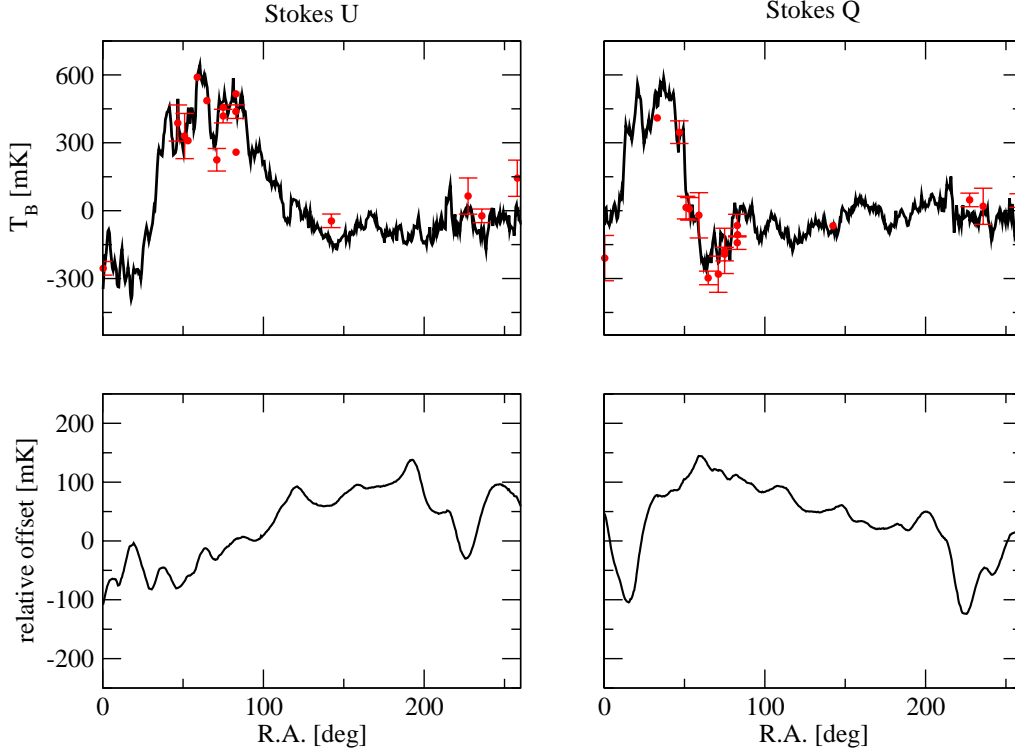


**Fig. 3.** Drift scan at  $56^\circ$  declination. The upper panels show Stokes  $U$  and  $Q$  brightness temperatures. Available data points from the Leiden/Dwingeloo survey are overlaid with error bars indicating the quoted errors. The lower panels show the relative system temperature derived from the de-stripping algorithm.

The digitized version of the Leiden/Dwingeloo data at 1.4 GHz provides Stokes  $U$  and  $Q$  brightness temperatures for more than 1600 different positions on the sky. About 700 positions are covered by our survey within a radius of  $15'$ . These common data points serve as reference values for the matrix fits discussed above. This means that our temperature scale fully relies on the Leiden/Dwingeloo data.

#### 4 Example Drift Scan

In Fig. 3 we show an example drift scan at  $56^\circ$  declination. The drift scan passes the *fan*-region, a bright, polarized region centered at about  $\alpha = 50^\circ$ ,  $\beta = 65^\circ$ . Considering the mean errors (60 mK as quoted for the Leiden/Dwingeloo data, and about 30 mK for the new survey), the Stokes  $U$  and  $Q$  distributions of both surveys are in good agreement for this drift scan. Remarkable is the appearance of small-scale structure which cannot be seen in the Leiden/Dwingeloo data set because of its coarse sampling. Fig. 3 also shows the offsets in Stokes  $U$  and  $Q$ , which apparently suffer from a temperature drift. This offset drift is most likely caused by variations of the receiver temperature or local environmental conditions and was derived from the de-stripping algorithm.

#### 5 Repeatability of Drift Scans

Repeatability of drift scans is an important criterion for accuracy. In Fig. 4 (top panels) we display two drift scans observed at the same declination ( $\delta = 40^\circ$ ). The repetition scan was observed 10 weeks later. Variations in the system temperature have been corrected as described above and are shown in the bottom panels of Fig. 4. Stokes  $U$  and  $Q$  values of both drift scans are in good agreement. The systematic difference in the relative offsets is caused by a change in the bandwidth of the IF-filters, and, as a result, the noise in all later drift scans decreased.

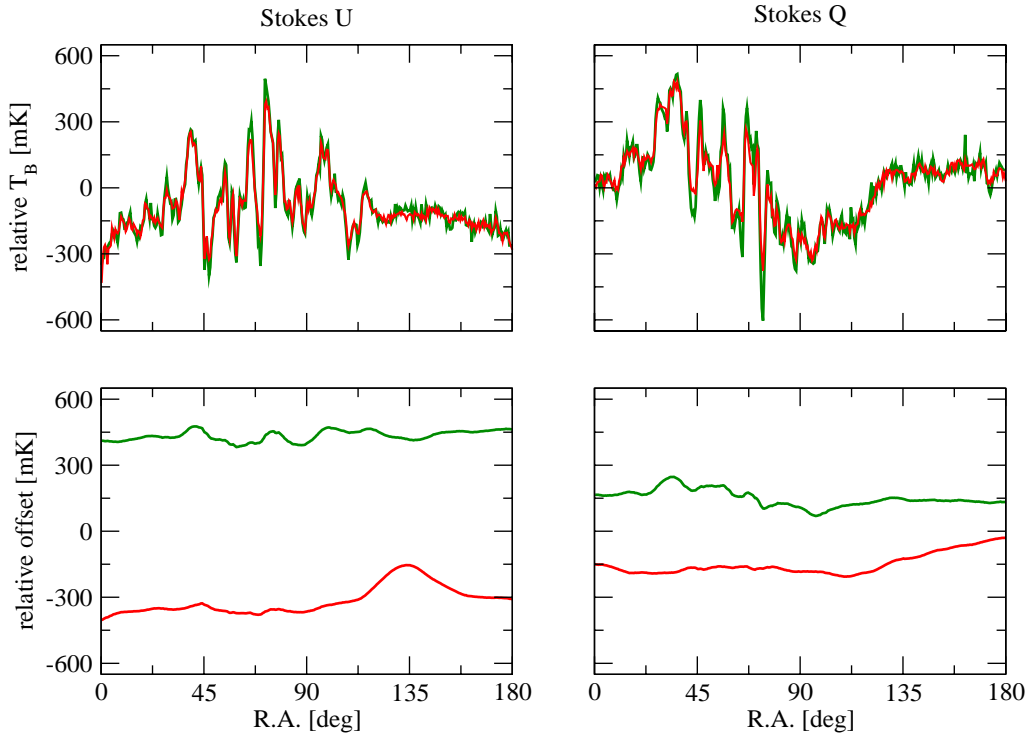


Fig. 4. Two drift scans at  $40^\circ$  declination observed on Nov. 20 (green) and Jan. 28, 2002 (red). The upper panels show brightness temperatures for Stokes  $U$  and  $Q$ . In the lower panels the relative system temperature is plotted.

## 6 Correlation of the DRAO and Leiden/Dwingeloo Polarization Survey

In the previous section a comparison of both surveys is made for a single scan at  $56^\circ$  declination. But how do the entire data sets compare? In Fig. 5 the correlation of polarized intensities is shown for all positions which are common to both surveys. Beside the linear correlation, a large scatter of polarized intensities is visible. The correlation coefficients for Stokes  $U$  and  $Q$  vary between 0.85 and 0.87 for this preliminary set of data. With an average error in the Leiden/Dwingeloo data of 60 mK, the error in our data thus results to about 30 mK.

## 7 Preliminary Map of Polarized Intensity

In Fig. 6 we show a preliminary map of the polarized intensity calculated by  $PI = \sqrt{U^2 + Q^2}$ . The Stokes  $U$  and  $Q$  data have been convolved to match a beam size of  $4^\circ$ . Two bright polarized regions of the northern sky are sticking out: the *fan*-region, and the north polar spur at  $\alpha = 230^\circ$ ,  $\delta = 18^\circ$ . It is planned to continue the observations to complete the sampling.

## References

- Brouw W. N., Spoelstra, T. A. T. (1976) *Astron. Astrophys. Suppl.* **26**, 129.  
 Duncan A. R., Haynes R. F., Jones K. L., Stewart R. T. (1997) *Mon. Not. R. Astron. Soc.* **291**, 279.  
 Junkes N., Fürst E., Reich W. (1987) *Astron. Astrophys. Suppl.* **69**, 451.  
 Reich W. (1982) *Astron. Astrophys. Suppl.* **48**, 210.  
 Reich P., Reich W. (1986) *Astron. Astrophys. Suppl.* **63**, 205.  
 Taylor A. R. et al. (2003) *Astron. J.* **125**, 3145.  
 Uyaniker B. et al. (1998) *Astron. Astrophys. Suppl.* **132**, 401.

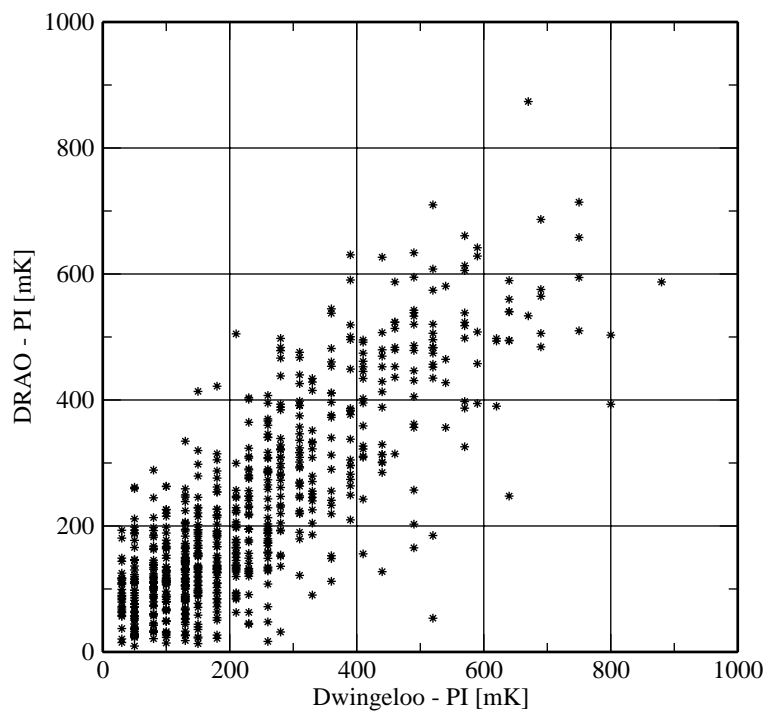


**Fig. 5.** Comparison of polarized intensities of the DRAO and Leiden/Dwingeloo polarization surveys.

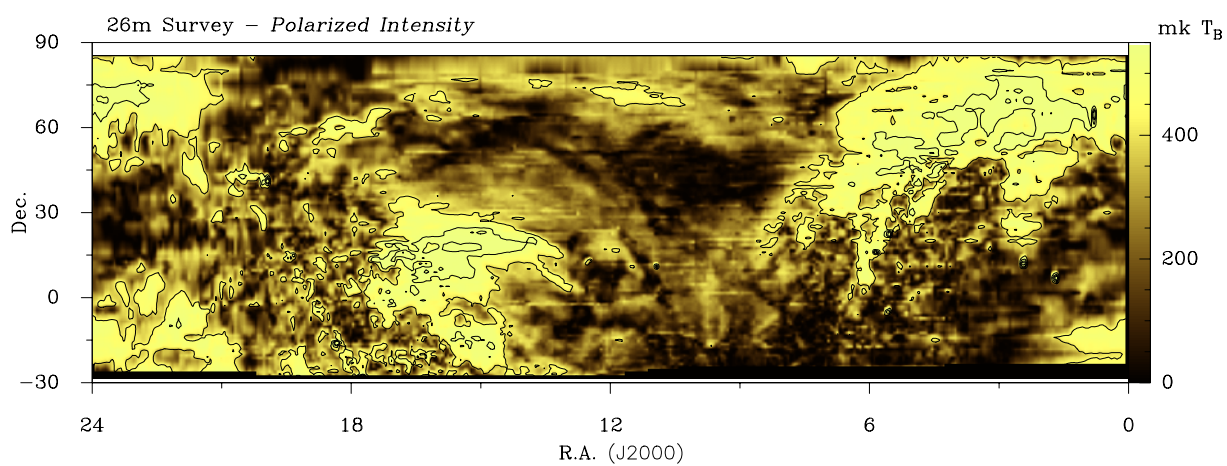


**Fig. 6.** Preliminary map of the polarized intensity. The original data have been convolved to match a beam size of  $2^\circ$ .

# A Large-Scale Radio Polarization Survey of the Southern Sky at $\lambda 21\text{cm}$

J.C. Testori<sup>1,2</sup>, P. Reich<sup>2</sup> and W. Reich<sup>2</sup>

<sup>1</sup>Instituto Argentino de Radioastronomía, C.C.5 (1894) Villa Elisa, Argentina

<sup>2</sup>Max-Planck-Institut für Radioastronomie, Auf dem Hügel 69, 53121 Bonn, Germany

**Abstract.** We have successfully reduced the polarization data from the recently published  $\lambda 21\text{cm}$  continuum survey of the southern sky carried out with a 30-m antenna at Villa Elisa (Argentina). We describe the reduction and calibration methods of the survey. The result is a fully sampled survey, which covers declinations from  $-90^\circ$  to  $-10^\circ$  with a typical rms-noise of 15 mK  $T_B$ . The map of polarized intensity shows large regions with smooth low-level emission, but also a number of enhanced high-latitude features. Most of these regions have no counterpart in total intensity and indicate Faraday active regions.

## 1 Introduction

Observations of linearly polarized radio emission provide valuable information about the Galactic magnetic field. For the southern sky, surveys at 408 MHz and 620 MHz are available which were carried out with the Parkes 64-m telescope (Mathewson & Milne 1965, Mathewson et al. 1966). These observations were made 40 years ago, and only recently polarization observations of the southern sky were continued at 2.3 GHz with the Parkes telescope (Duncan et al. 1997) and at 1.4 GHz with ATCA (Gaensler et al. 2001). However, these high-frequency observations are limited to measurements along the Galactic plane so far. Large-scale information is missing and the polarization structures at high latitudes are not observed.

For the northern hemisphere a number of large-scale surveys of linear polarization is available, which were carried out with the Dwingeloo 25-m telescope (Brouw & Spoelstra 1976). Their highest frequency survey was at 1.411 GHz with an angular resolution of about  $35'$ . This survey is absolutely calibrated and corrected for all kinds of instrumental effects. However, the data are largely under-sampled and the sensitivity is low. In this paper we describe a complete, regularly gridded polarization survey of the southern sky at 1.435 GHz with similar angular resolution.

## 2 Observations

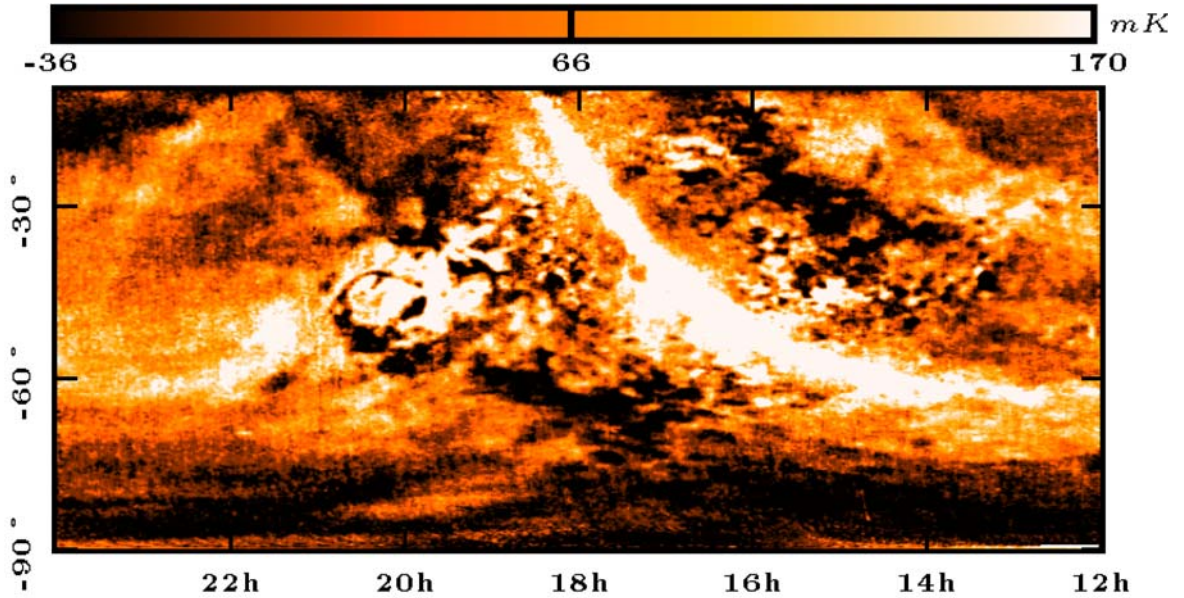
The polarization observations presented here were made using one of the two 30-m telescopes of the Instituto Argentino de Radioastronomía in Villa Elisa as part of a continuum survey carried out in collaboration with the MPIfR in Bonn. The total intensity survey (Reich et al. 2001) was absolutely calibrated by sky horn measurements, has an angular resolution of  $35'.9$  and a sensitivity of 50 mK ( $3 \times r.m.s.$ ) in full beam brightness temperature  $T_B$ .

For the survey observations the telescope was equipped with a two channel receiver, which was connected to an IF-polarimeter. The left-hand and right-hand circularly polarized signals were correlated to obtain signals corresponding to linear polarization parameters Stokes  $U$  and  $Q$  in the instrumental reference frame. Simultaneously, two total power (LHC and RHC) channels were recorded. The system noise was approximately 90 K in both channels. Details of the receiving system were already given by Testori et al. (2001). All basic parameters of the survey are listed in Table 1.

The observations were realized by applying the *"Nodding Scan Technique"* (Haslam et al. 1974), where the telescope moves continuously along declination in the local meridian. Up and down scans

**Table 1.** Parameters of the Villa Elisa Polarisation Survey

Coverage	$0^{\text{h}} \leq \alpha \leq 24^{\text{h}}$ $-90^{\circ} \leq \delta \leq -10^{\circ}$
$T_{\text{sys}}$	90 K
HPBW	35'9
Centre frequency	1435 MHz
Bandwidth	14 MHz
Sensitivity in $U, Q$	<i>r.m.s.</i> $\simeq$ 15 mK
Polarization angle error	$\pm 3^{\circ}$
Pointing accuracy	$\pm 2'$

**Fig. 1.** The original Stokes parameter  $U$  at 1.435 GHz. The angular resolution is 35'9.

were recorded and the earth rotation provides a full coverage in right ascension. Each day the observations were started 1 minute later in sidereal time to provide a full sampling after 16 nights. The telescope moved with a speed of  $10^{\circ}$  per minute in the declination range between  $-90^{\circ}$  and  $-10^{\circ}$ . A full sampling of  $0^{\circ}.25$  in both coordinates was obtained. Each up or down scan was observed at least twice.

### 3 Data reduction and ground radiation determination

In a first step the two polarization channels of more than 16000 scans were edited for all kinds of interference following the methods applied for the total-intensity data (Testori et al. 2001). The mean intensity level for each  $U$  and  $Q$  scan was set to zero. Scanning effects in the maps were suppressed by using the method of unsharp masking (Sofue & Reich 1979). The determination of an elevation-dependent ground radiation is complicated because the distribution of polarized high-latitude emission is entirely unknown. We applied the "BackGround Filtering Technique" (BGF) by Sofue & Reich (1979) using a  $10^{\circ} \times 6^{\circ}$  wide filter in right ascension and declination, respectively. Excluding all small-

scale emission we find the mean large-scale polarization for each polarization channel as a function of elevation. This was interpreted as the contribution from the ground, which was subtracted for each scan. Up and down scans were treated separately. The final *r.m.s.*-noise in the maps was measured to be approximately 15 mK in *U* and *Q*.

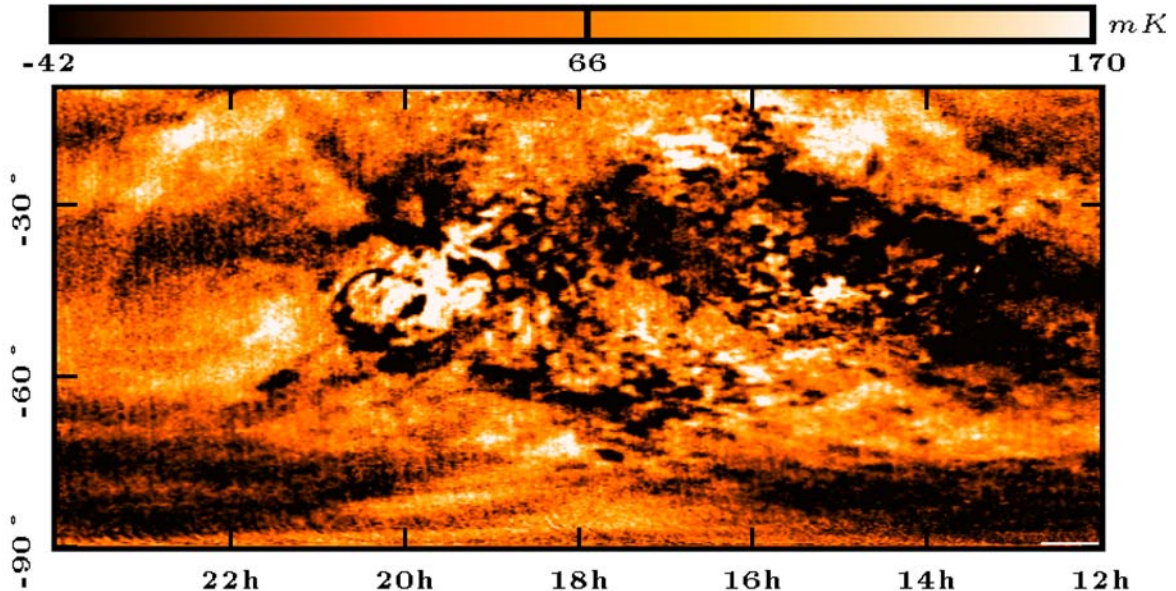


Fig. 2. Same as Fig. 1, but corrected for instrumental polarization.

#### 4 Instrumental polarization

The most severe instrumental problem of this polarization survey is the cross-talk from the total-intensity channels into the polarization channels. We found an overall value of 8.8%, corresponding in that case to 4.9% for Stokes *U* and 7.3% for Stokes *Q*. Figure 1 shows the polarization channel Stokes *U* (in the instrumental frame) including instrumental polarization. Figure 2 shows the same polarization channel after subtraction of the appropriately scaled total-power map. The Galactic plane is dominating the uncorrected data (Fig. 1), whereas it becomes nearly invisible with remaining patchy emission structures after the appropriate correction.

#### 5 Polarization angle

To derive the instrumental correction of the polarization angles, we used a number of strong polarized sources previously observed at 1.4 GHz with the Parkes 64-m telescope: the radio galaxies Fornax A, Pictor and in particular the highly polarized source Centaurus A.

Figure 3 shows the comparison of the Villa Elisa data and the Parkes 1.4 GHz map (Junkes, private communication) for Centaurus A. The instrumental angle correction we applied results in angle differences to the Parkes data in the range of  $\pm 3^\circ$ , which we adopt as our systematic polarization angle accuracy.

#### 6 Zero-level

The polarization survey needs to be adjusted to an absolute zero-level. Absolute polarization data, however, are not available for the southern sky at 1.4 GHz and low-frequency extrapolations are

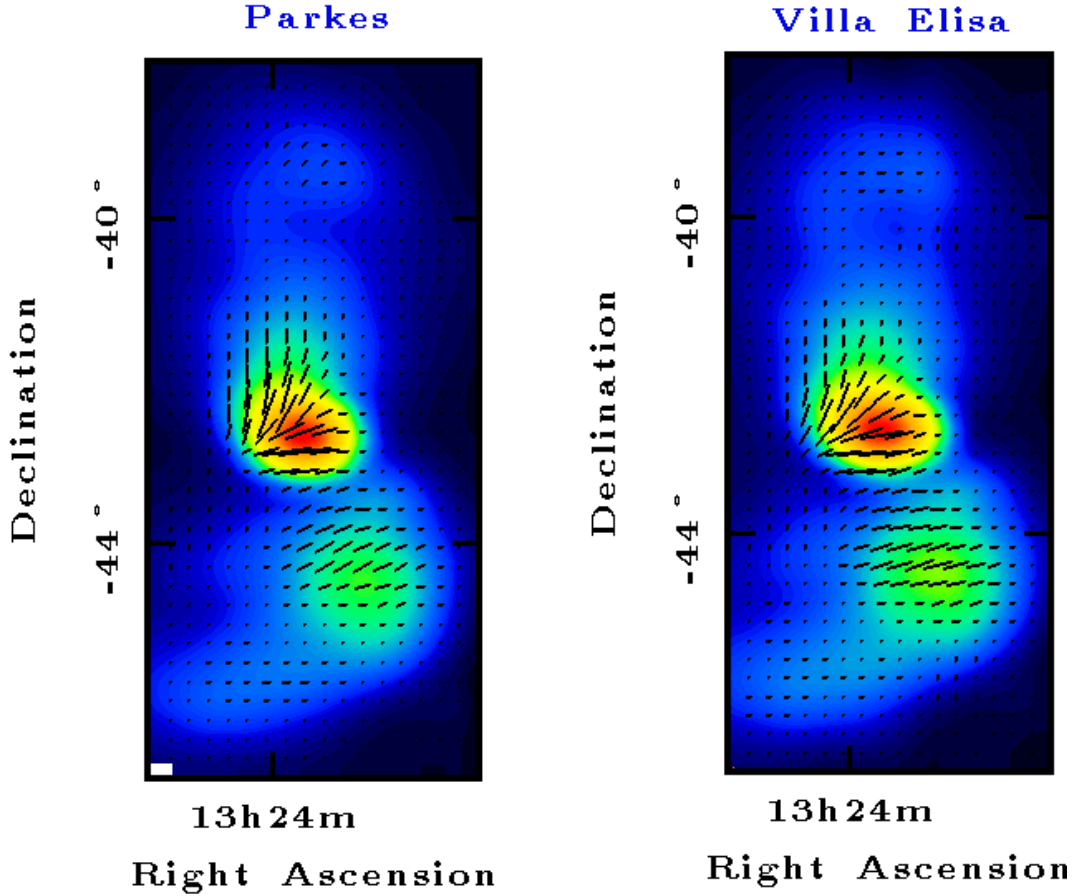


**Fig. 3.** The left panel shows the 1.4 GHz map of the radio galaxy Centaurus A observed with the Parkes 64-m telescope convolved to a HPBW of  $35''.9$ . The right panel shows the Villa Elisa data. Both panels display total intensities with superimposed polarization vectors in the B-field direction (assuming no Faraday rotation). The length of each vector is proportional to the polarized intensity at each point.

quite uncertain. We will adjust the Villa Elisa southern-sky survey by using the recent northern-sky polarization data at 1.4 GHz carried out with the 26-m antenna at DRAO by Wolleben et al. (this volume), which are absolutely calibrated. Both surveys overlap in the area from declination  $\delta = -28^\circ$  to about  $\delta = -10^\circ$ .

## 7 Preliminary results

The polarization survey shows large regions with smooth low-level emission, but also a number of enhanced high-latitude features. Most of these regions have no counterpart in total intensity, even when the large-scale component has been removed, which might mask small-scale emission. This indicates the presence of Faraday active regions.

Figure 4 shows the distribution of the polarization angles for the area  $12^{\text{h}} \leq \alpha \leq 24^{\text{h}}$ , and  $-90^\circ \leq \delta \leq -10^\circ$  with large coherent structures, but also regions with strong fluctuations. Figure 5 details one of these high-latitude structures. The total power map shows smooth low-level structures, while the Stokes  $U$  map shows large intensity fluctuations. These are also reflected in the polarized intensity map with superimposed polarization vectors. The enhanced polarization structure has a size of approximately  $17^\circ \times 20^\circ$ . This indicates local Faraday rotation of distant polarization as frequently discussed during this conference.

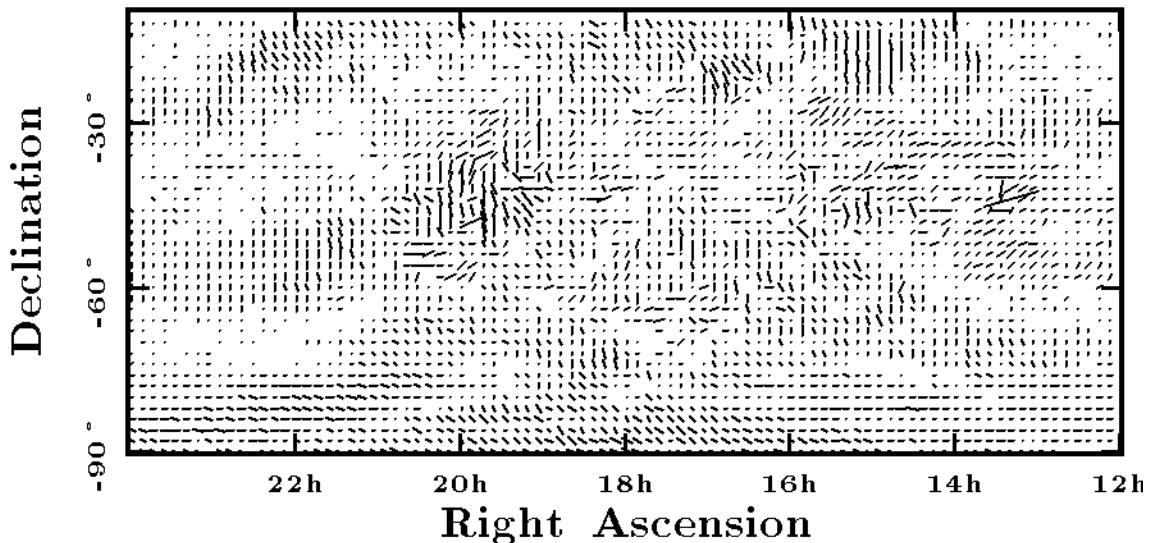


Fig. 4. Magnetic B-field vectors at 1.435 GHz (assuming no Faraday rotation). Every eight's vector is shown.

## 8 Final remarks

We briefly described the observation, reduction and calibration of the 1.435 GHz southern polarization survey carried out with the Instituto Argentino de Radioastronomía 30-m antenna in Villa Elisa. The maps shown are on a relative level but will be absolutely calibrated with data from the recent DRAO northern-sky polarization survey (Wolleben et al., this volume). This  $\lambda 21\text{cm}$  polarization survey is the first one covering the entire southern sky and its frequency and angular resolution is the highest among all southern large-scale surveys outside of the Galactic plane.

## Acknowledgments

We are grateful to Drs. Norbert Junkes and Ray Haynes for providing the Parkes 1.4 GHz data of Centaurus A prior to publication. JCT likes to thank Prof. Richard Wielebinski for financial support and Gabi Breuer for assistance when preparing the manuscript.

## References

- Brouw W. N., Spoelstra T. A. Th. (1976) *Astron. Astrophys. Suppl. Ser.* **26**, 129.  
 Duncan A. R., Haynes R. F., Jones K. L., Stewart R. T. (1997) *Mon. Not. R. Astron. Soc.* **291**, 279.  
 Gaensler B. M., Dickey J. M., McClure-Griffiths N. M. et al. (2001) *Astrophys. J.* **549**, 959.  
 Haslam C. G. T., Wilson W. E., Graham D. A., Hunt C. G. (1974) *Astron. Astrophys. Suppl. Ser.* **13**, 359.  
 Mathewson D. S., Broten N. W., Milne D. K. (1966) *Aust. J. Phys.* **19**, 93.  
 Mathewson D. S., Milne D. K. (1965) *Aust. J. Phys.* **18**, 635.  
 Reich P., Testori J. C., Reich W. (2001) *Astron. Astrophys.* **376**, 861.  
 Sofue Y., Reich W. (1979) *Astron. Astrophys.* **38**, 251.  
 Testori J. C., Reich P., Bava J. A. et al. (2001) *Astron. Astrophys.* **368**, 1123.

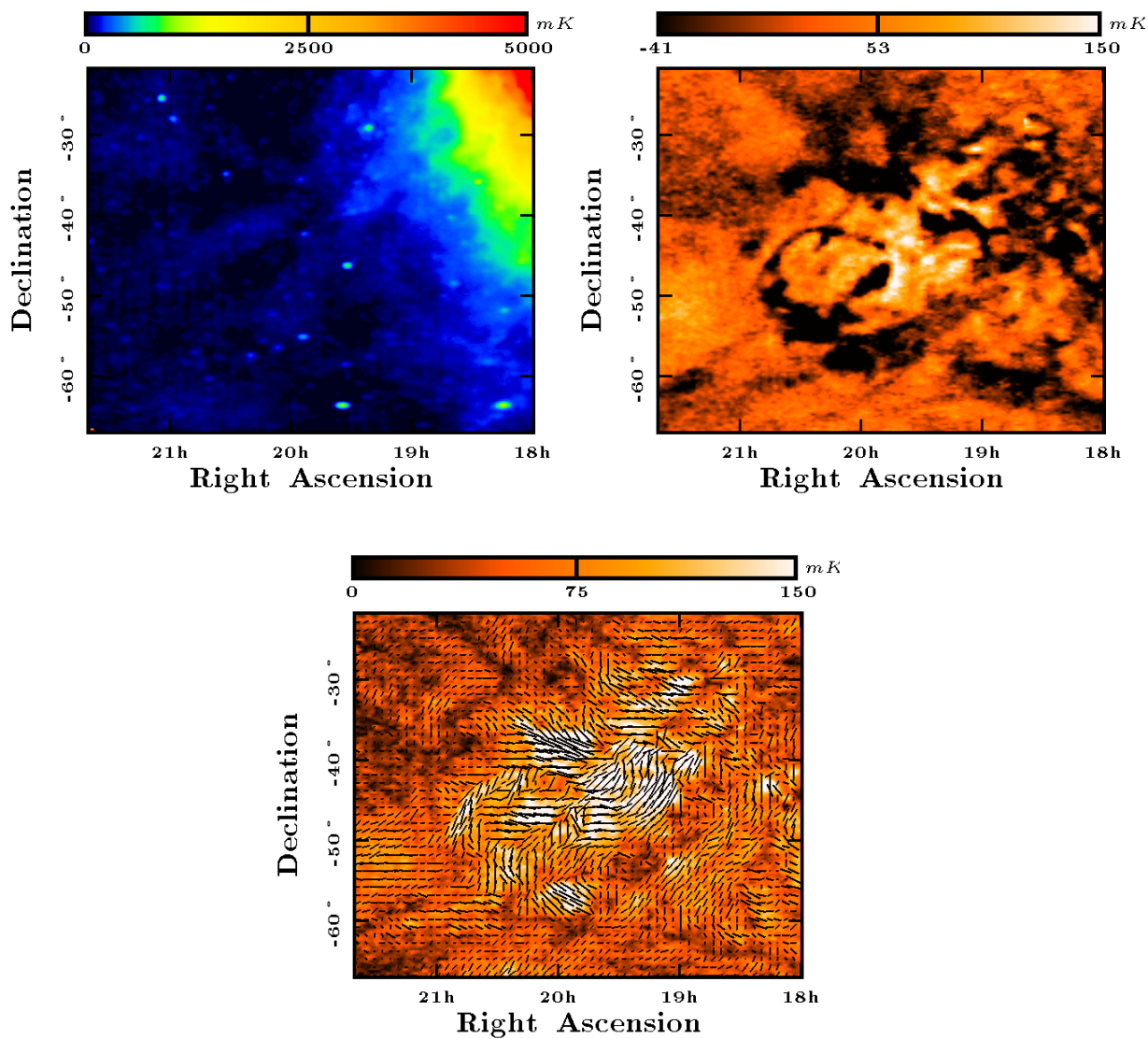


**Fig. 5.** Maps of a field centered at  $\alpha = 19^{\text{h}}50^{\text{m}}$ ,  $\delta = -44^{\circ}30'$  ( $l \sim 335^{\circ}$ ,  $b \sim -29^{\circ}$ ). The upper left panel shows the total intensity map with the large-scale component removed. The upper right panel shows the Stokes parameter  $U$  map for the same area. Bottom: The polarized intensity image with superimposed polarization vectors in the E-field direction. The length of each vector is proportional to the polarized intensity at each point. Every fourth vector is shown.

## Spectral Index Variations of Galactic Emission

P. Reich<sup>1</sup>, W. Reich<sup>1</sup> and J.C. Testori<sup>2</sup>

<sup>1</sup> Max-Planck-Institut für Radioastronomie, Auf dem Hügel 69, 53121 Bonn, Germany

<sup>2</sup> Instituto Argentino de Radioastronomía, C.C. 5, 1894 Villa Elisa (Prov. de Bs.As.), Argentina

**Abstract.** We have used all-sky maps at 45 MHz, 408 MHz, 1420 MHz and 22.8 GHz to calculate the distribution of spectral indices across the sky. This requires an adjustment of the adopted zero-levels of the different surveys, which was performed by temperature-versus-temperature (TT) plots. While at high frequencies a spectral steepening with increasing Galactic latitude is seen in the same way as it is observed in nearby galaxies seen edge-on, the spectral index distribution is more complex at lower frequencies. In general there is an agreement with the cooling-convection halo models by Lerche & Schlickeiser (1982), but also local magnetic field variations and variations of the cosmic-ray electron energy spectrum may explain the distribution of low-frequency spectral indices.

### 1 Introduction

Radio continuum surveys have been carried out since the early days of radio astronomy (see Wielebinski, this volume). They are the basis to derive the general properties of the Galaxy, e.g. the size of its thin and thick disk (halo), its magnetic fields strength and structure and to trace sites of thermal and synchrotron sources and source complexes. By comparing radio surveys at several frequencies a separation of Galactic thermal and non-thermal emission is possible and the energy spectrum of synchrotron emitting electrons can be derived. The precise knowledge of the spectral behaviour of Galactic emission is also of importance to estimate its intensity and structure at high frequencies, where studies of the fluctuations of the cosmic microwave background (CMB) were made.

However, all-sky survey observations are rare as they are time consuming. In addition they need to be absolutely calibrated with well adjusted scales and zero-levels to be useful for a reliable spectral index determination. These requirements are sometimes difficult to achieve.

### 2 Survey data used

The all-sky surveys included in this spectral index study are: the southern-sky survey at 45 MHz (Alvarez et al. 1997) and the northern-sky survey at 46.5 MHz (Maeda et al. 1999), the 408-MHz all-sky survey by Haslam et al. (1982), the southern-sky survey (Reich et al. 2001) and the northern-sky survey (Reich 1982, Reich & Reich 1986) at 1420 MHz, and the recent 22800-MHz WMAP survey (Bennett et al. 2003a).

The combined 45-MHz map has an angular resolution of  $5^\circ$  and all other surveys were convolved to that resolution. Detailed information about the low-frequency surveys was given by Reich (2003). As an example for all-sky surveys we display the 1420-MHz map in Fig. 1. The maximum emission along the Galactic plane reflects the high concentration of emission in the Galactic disk. At  $5^\circ$  angular resolution most source complexes merge with the diffuse unresolved emission, however, the local spiral arm towards Cygnus and Vela (longitudes close to  $90^\circ$  and  $270^\circ$ , respectively) clearly show up. The most intense feature sticking out of the Galactic plane from about  $30^\circ$  longitude to about  $80^\circ$  latitude is the North Polar Spur (NPS), likely a nearby old supernova remnant.

### 3 Basic relations

The following relations are used:

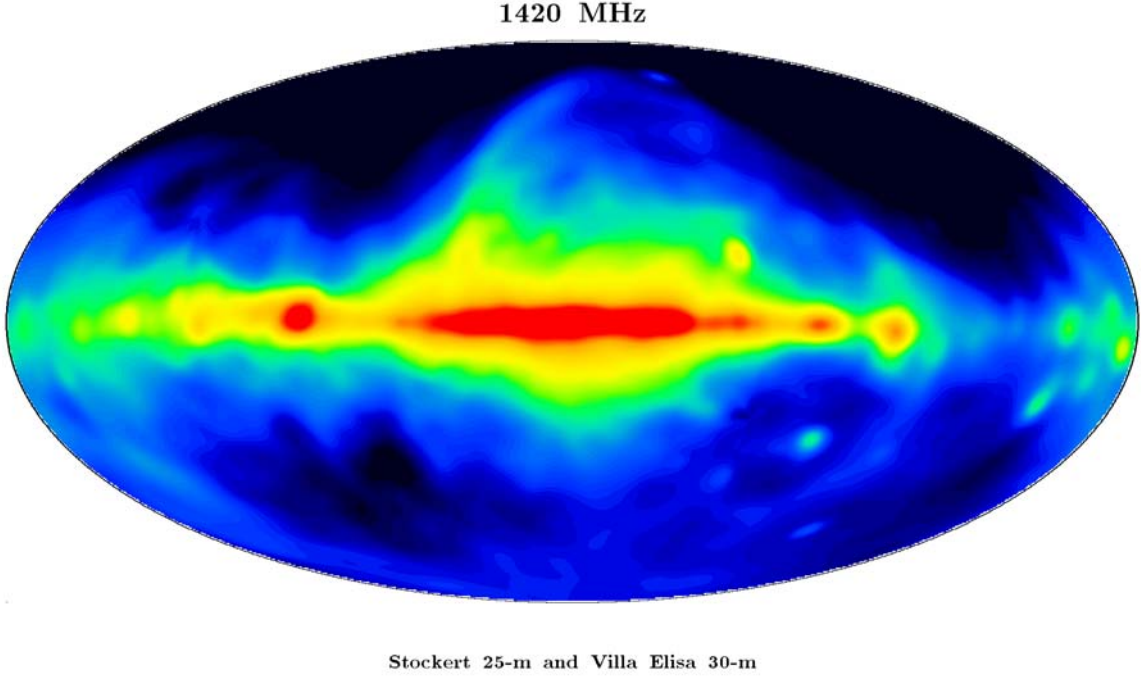


**Fig. 1.** 1420-MHz all-sky map in Galactic coordinates at a resolution of  $5^\circ$ . The colour coding is linear from dark blue to red representing 3.4 K to 8.0 K.

The *temperature spectral index*  $\beta$  is defined as :

$$\beta = -\frac{\log(T_1/T_2)}{\log(\nu_1/\nu_2)} \quad (1)$$

with  $T_i$  = Galactic brightness temperature at frequency  $\nu_i$ . The *flux density spectral index*  $\delta$  is related to  $\beta$  as:

$$\delta = \beta - 2. \quad (2)$$

The observed temperature  $T_{\text{OBS}}$  consists of

$$T_{\text{OBS}} = T_{\text{GAL}} + T_{\text{CMB}} + T_{\text{EX}} + T_{\text{OFF}} \quad (3)$$

with

$T_{\text{GAL}}$  = Galactic brightness temperature

$T_{\text{CMB}}$  = cosmic microwave background = 2.73 K (Mather et al. 1994)

$T_{\text{OFF}}$  = zero-level error

$T_{\text{EX}}$  = contribution of unresolved extragalactic sources where

$$T_{\text{EX}} = 30 \text{ K} \cdot \left( \frac{\nu}{178 \text{ MHz}} \right)^{-2.9}. \quad (4)$$

The value of  $30 \pm 7$  K has been taken from Bridle (1967), who determined the temperature spectral index to be 2.75 for the frequency range between 13 and 404 MHz. However, recently Zhang et al. (2003) found a mean flux density spectral index of  $\delta = 0.9$  between 327 MHz and 1400 MHz.

#### 4 Zero-level determination

From eq. 3 it is clear that for the determination of the spectral index distribution of Galactic emission  $T_{\text{GAL}}$  the unwanted contributions  $T_{\text{CMB}}$ ,  $T_{\text{EX}}$  and  $T_{\text{OFF}}$  have to be subtracted.  $T_{\text{OFF}}$  has the largest

uncertainty, but also the largest influence on the spectral index result in particular at high frequencies. We used the methods of TT-plots (temperature-versus-temperature plot) in order to derive the relative offsets between all surveys (for details see Reich & Reich 1988a). All maps have been convolved to a common resolution of  $15^\circ$  in equatorial coordinates. The undisturbed area between the intense local objects Loop I (NPS) and Loop III, which is the declination range between  $30^\circ$  and  $45^\circ$ , was selected for TT-plots in order to compare the results with those of Reich & Reich (1988a). Data from the Galactic plane region was omitted for the analysis. At one frequency, we choose 1420 MHz, the zero-level needs to be fixed. We set 2.8 K for the sum of  $T_{\text{CMB}}$  and  $T_{\text{EX}}$  at 1420 MHz. The extrapolated spectral index fit then gives a temperature offset for the other frequency. This extrapolation assumes a constant spectral index for all emission in this section of the sky. Figure 2 shows the scheme of the determination of  $T_{\text{OFF}}$ , and Table 1 lists the results.

Absolute zerolevel determination by temperature–temperature plots (TT–plots)

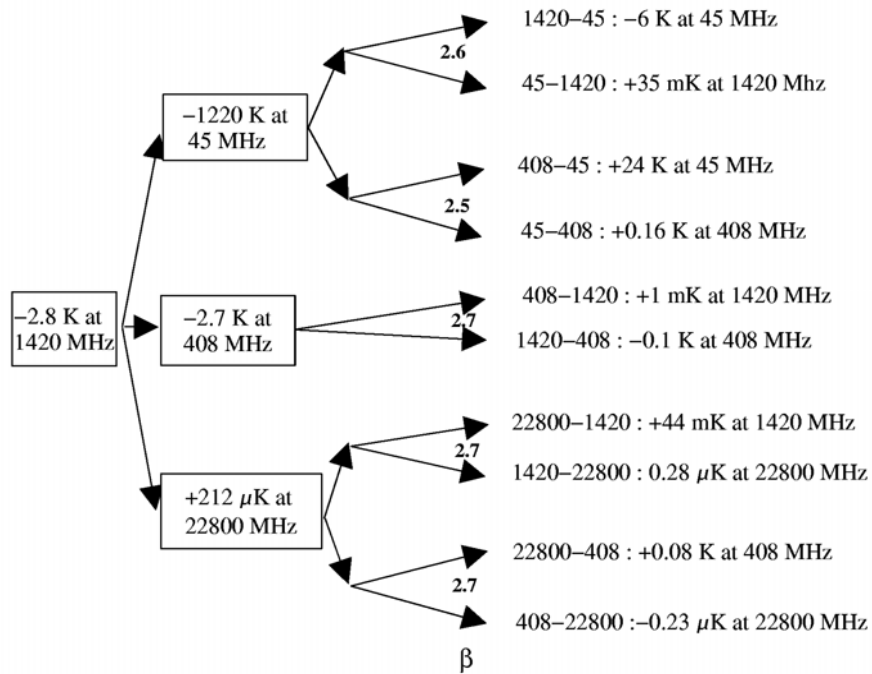


**Fig. 2.** Scheme of the determination of absolute zero-levels. The spectral index fitted for the selected strip of sky is given. The residual offsets left indicate a high degree of consistency.

By the TT-plots the absolute zero-levels of the four surveys are fixed with quite small errors as given in Fig. 2. All derived zero-level corrections are within the cited zero-level error (see Table 1), when at 45 MHz the error for  $T_{\text{EX}}$  is included. At 45 MHz  $T_{\text{EX}}$  depends also strongly on  $\beta$  so that we also give the value for  $\beta = 2.75$  in Table 1.

## 5 Results

The resulting spectral index maps show the spectrum of the Galactic emission, which is a mixture of synchrotron emission and thermal emission. The 45–408-MHz spectral index map will be discussed elsewhere. Spectra are in general flatter than at higher frequency due to the well-known flattening of the Galactic electron spectrum at low energies (see below).

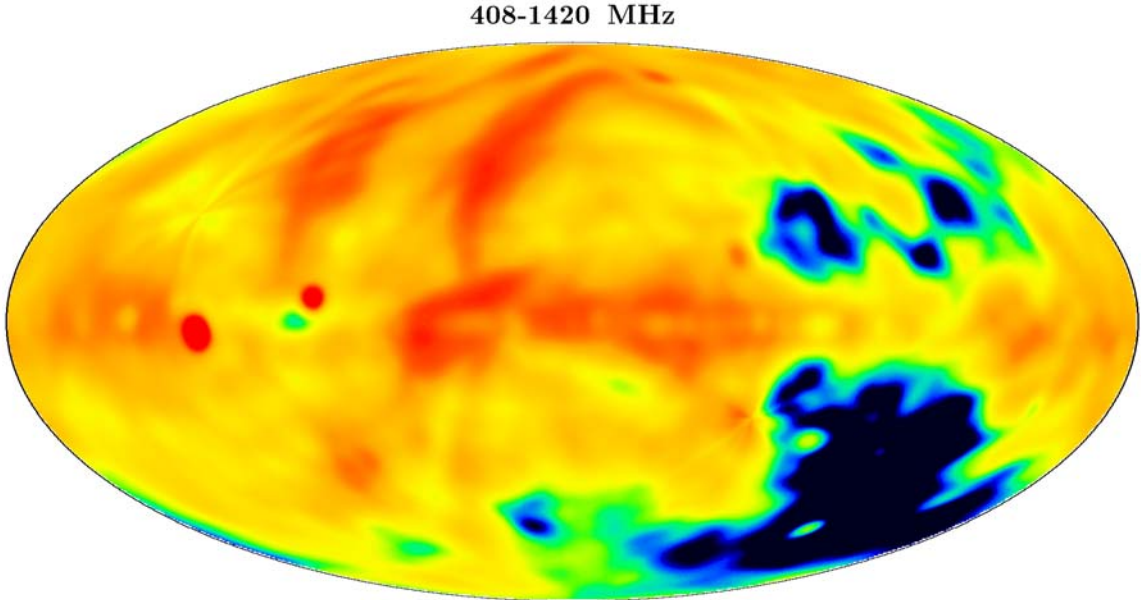
Figures 3 and 4 show the 408–1420-MHz spectral index map and the 1420–22800-MHz spectral index map, respectively. The colour coding is always the same, running from dark blue (spectral index

**Table 1.** Results of the TT-plots

Frequency	$T_{\text{OFF+EX+CMB}}$ from TT-plots	$T_{\text{EX+CMB}}$ theoretically	$T_{\text{OFF}}$	$\pm T_{\text{ZERO}}$ as quoted
45 MHz	1220±15 K	1621±378 K	−399 K	100 K
		1319±307 K*	−99 K*	100 K
408 MHz	2.7±0.1 K	5.4±0.6 K	−2.7 K	3.0 K
1420 MHz	2.8±0.035 K	2.8±0.02 K	0.0 K	0.5 K
22800 MHz	−212±0.25 $\mu$ K	2.73 K + 23±5 $\mu$ K	—	not given

\*extrapolation of  $T_{\text{EX}}$  based on  $\beta = 2.75$  instead of  $\beta = 2.9$ , see text

of 2.4) and to red (spectral index of 3.0), representing areas with a steep spectrum. Yellow shows spectral indices of 2.6, orange of 2.7.

**Fig. 3.** Spectral index map between 408 MHz and 1420 MHz.

Spectral index variations are visible all over the sky. Flat-spectrum areas are found in the Galactic plane, where thermal disk emission (Fig. 4) or H II regions (Fig. 3) are significant components.

The 408–1420-MHz spectral-index map (Fig. 3) shows the NPS (Loop I) and Loop III as high latitude steep-spectrum features. A steep-spectrum 'halo' component is limited to  $\pm 60^\circ$  in longitude and  $\pm 15^\circ$  in latitude. Towards the anti-centre the spectra flatten significantly towards higher latitudes. This behaviour was already noted by Reich & Reich (1988a) for positive latitudes in the spectral-index map of the northern sky, but is also seen for negative latitudes based on independent southern-sky data.

The 1420–22800-MHz spectral-index map shows rather flat spectra along the Galactic plane due to the dominance of thermal disk emission and steep spectra outside. Some large thermal complexes like the Gum Nebula, the Orion region and the Ophiuchus complex north of the Galactic centre show up as high latitude flat-spectrum areas.

From the comparison of the spectral-index maps covering a wide frequency range a complex be-

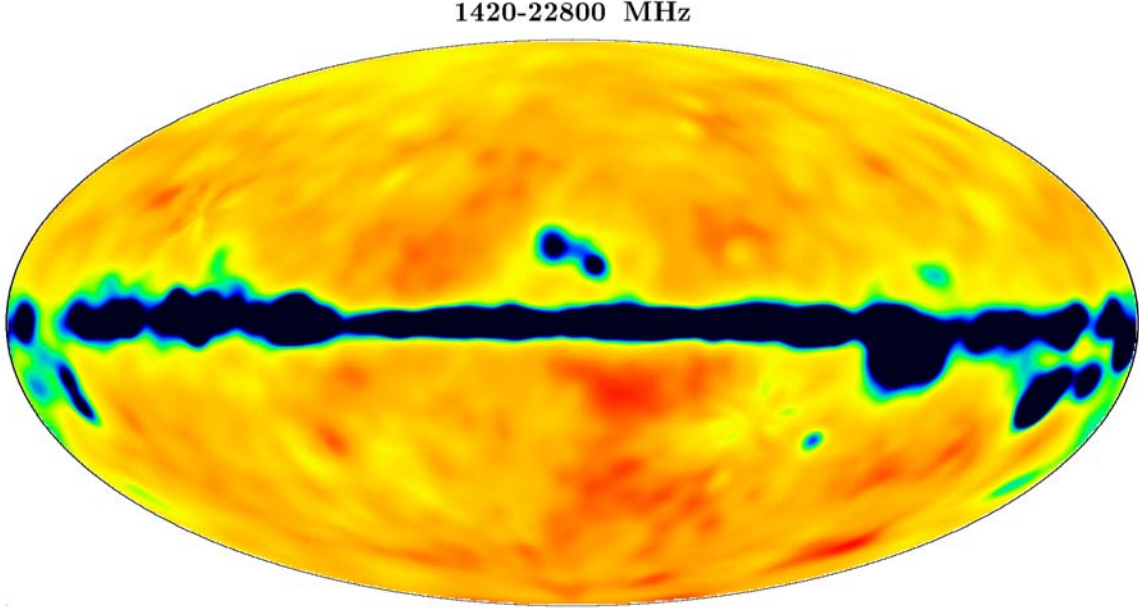


Fig. 4. Spectral index map between 1420 MHz and 22800 MHz.

behaviour of Galactic spectral indices is evident: a general steepening with frequency and significant variations across the sky. This implies that an extrapolation over a wide frequency range is quite uncertain.

## 6 Discussion

The cosmic-ray electron spectrum (e.g. Fulks 1975, his Fig. 10) shows a clear bend with energy  $E$ :  $p \approx 2.3$  at 1 GeV and  $p \approx 3.3$  at 100 GeV (Webber 1983) with  $E^{-p}$ . Other measurements report values of  $p \approx 3.6 \pm 0.2$  (6–35 GeV, Boezio et al. 2000) or  $p \approx 3.15 \pm 0.13$  (4–26 GeV, Golden et al. 1994). This bend reflects the general steepening of the Galactic spectrum with frequency. For a certain observing frequency  $\nu$  the electron energy  $E$  and magnetic field component  $B_{\perp}$  calculate by:

$$\nu = 16 \cdot B_{\perp} (\mu\text{G}) \cdot E^2 (\text{GeV}) . \quad (5)$$

Locally we have  $B_{\perp} \sim 5 \mu\text{G}$  (Strong et al. 2000), so that at 45 MHz electrons of 0.75 GeV are observed, at 408 MHz those with 2.26 GeV, at 1420 MHz with 4.21 GeV, and at 22800 MHz with 16 GeV.

Reich & Reich (1988b) have already discussed the spectral flattening towards higher latitudes in the anti-centre area together with the steep-spectrum ‘halo’ in the inner Galaxy in terms of the cooling-convection models by Lerche & Schlickeiser (1982), which are based on the existence of a Galactic wind. These models predict spatial variations of the non-thermal spectral index with  $z$ , which depend on the energy spectrum of the injected electrons in the plane  $E^{-p}$  ( $p > 1$ ) and an energy-dependent diffusion coefficient ( $D \propto E^a$  with  $0 \leq a < 1$ ). Figure 5 summarizes their result for the synchrotron spectral index  $\delta$ . Below the critical frequency  $\nu_C(E_D)$  (with the characteristic energy  $E_D$  depending on the Galactic wind speed),  $\delta$  decreases at a certain  $z$  by  $a(4 + a + 2p)/(24 + 4a)$  (spectral flattening), above  $\nu_C$   $\delta$  increases by  $0.5(p - 1)$  (spectral steepening). At low  $z$  in the Galactic plane the spectrum steepens by  $\delta = 0.25$  above the critical frequency  $\nu_C$ . The spectral index results between 408–1420 MHz indicate that in the anti-centre area in general we have conditions below  $\nu_C$ , while in the central Galactic area they are above  $\nu_C$ . Spectral indices between 1420–22800 MHz indicate a steepening out of the plane everywhere or conditions above  $\nu_C$ .

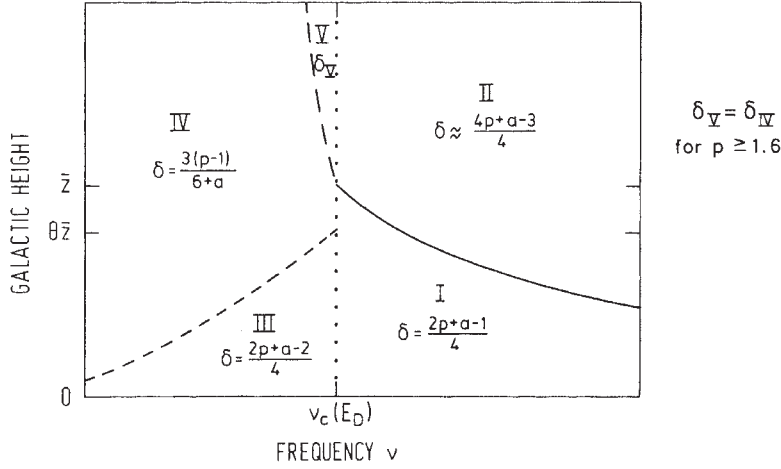


**Fig. 5.** Spatial variations of the synchrotron flux density spectral index  $\delta$  according to the model of Lerche & Schlickeiser (1982, their Fig. 2).

Assuming  $a=0.5$  and  $p$  between 2.3 and 3.3 for the observed high and low electron energy spectra we calculate a spectrum flattening between 0.18 and 0.21 towards high latitudes below  $\nu_C$  and a steepening between 0.65 and 1.15 above  $\nu_C$ . The predicted spectrum flattening is in good agreement with the observed spectra in the anti-centre direction. The predicted steepening is quite high when compared to the observations, although the model predictions are valid only for the synchrotron component, while the spectral-index maps include thermal emission.

A different explanation of the spectral characteristics is based on observational evidence for excessive local synchrotron emission (e.g. Wolleben & Reich 2004). In case the excess is based on quite local enhanced magnetic fields (within about 100 pc) flat-spectrum emission from electrons of low energy may have an influence for large areas of the sky with low emission, which is the case for high latitudes in the anti-centre direction.

A more detailed report of this investigation will be given elsewhere (Reich et al., in preparation).

## Acknowledgments

JCT is grateful to Prof. Richard Wielebinski for financial support.

## References

- Alvarez H., Aparici J., May J., Olmos F. (1997) *Astron. Astrophys. Suppl.* **124**, 315.  
 Bennett C.L., Halpern M., Hinshaw G. et al. (2003) *Astrophys. J. Suppl.* **148**, 1.  
 Boezio M., Carlson P., Francke T. et al. (2000) *Astrophys. J.* **532**, 653.  
 Bridle A.H. (1967) *Mon. Not. R. Astron. Soc.* **136**, 219.  
 Fulks G.J. (1975) *J. Geophys. Res.* **80**, 1701.  
 Golden R.L., Grimani C., Kimbell B.L. et al. (1994) *Astrophys. J.* **436**, 769.  
 Haslam C.G.T., Stoffel H., Salter C.J., Wilson W.E. (1982) *Astron. Astrophys. Suppl.* **47**, 1.  
 Lerche I., Schlickeiser R. (1982) *Astron. Astrophys.* **107**, 148.  
 Maeda K., Alvarez H., Aparici J., May J., Reich P. (1999) *Astron. Astrophys. Suppl.* **140**, 145.  
 Mather J.C., Cheng E.S., Cottingham D.A. et al. (1994) *Astrophys. J.* **420**, 439.  
 Reich P., Reich W. (1986) *Astron. Astrophys. Suppl.* **63**, 205.  
 Reich P., Reich W. (1988a) *Astron. Astrophys. Suppl.* **74**, 7.  
 Reich P., Reich W. (1988b) *Astron. Astrophys.* **196**, 211.  
 Reich P., Testori J.C., Reich W. (2001) *Astron. Astrophys.* **376**, 861.  
 Reich P. (2003) *Acta Astronomica Sinica Suppl.* **44**, 130.  
 Reich W. (1982) *Astron. Astrophys. Suppl.* **48**, 219.  
 Strong A.W., Moskalenko I.V., Reimer O. (2000) *Astrophys. J.* **537**, 763.  
 Webber W.R. (1983) in *Composition and Origin of Cosmic Rays*, ed. M.M. Shapiro, D. Reidel Publ. Comp., p. 83.  
 Wolleben M., Reich W. (2004) *Astron. Astrophys.*, submitted.  
 Zhang X., Reich W., Reich P., Wielebinski R. (2003) *Astron. Astrophys.* **404**, 57.